Supporting Information

Global Models Underestimate Large Decadal Declining and Rising Water Storage Trends Relative to GRACE Satellite Data

Bridget R. Scanlon, Zizhan Zhang, Himanshu Save, Alexander Y. Sun, Hannes Müller Schmied, Ludovicus P.H. van Beek, David N. Wiese, Yoshihide Wada, Di Long, Robert C. Reedy, Laurent Longuevergne, Petra Döll, and Marc F.P. Bierkens

Contents

List of Figures

List of Tables

Acronyms

CLM: Common Land Model or Community Land Model
CLSM: Catchment Land Surface Model
CMAP: NOAA Climate Prediction Center Merged Analysis of Precipitation
CRU: Climate Research Unit
CSR-M: University of Texas Center for Space Research Mascons GRACE solution
CSRT-GSH.sf: Univ. of Texas Center for Space Research Tellus Gridded Spherical Harmonic GRACE solution, rescaled (sf, scaling factor)
ET: evapotranspiration
EX: extraction of water
FAO: Food and Agricultural Organization
GDP: gross domestic product
GHM: global hydrologic model
GHWRM: Global hydrologic and water resource models
GLDAS: Global Land Data Assimilation System
GMSL: global mean sea level
GPCC: Global Precipitation Climatology Centre
GRACE: Gravity Recovery and Climate Experiment
GRDC: Global Runoff Data Centre
GWS: groundwater storage
IPCC: Intergovernmental Panel on Climate Change
ISI-MIP: Inter-Sectoral Impact-Model Intercomparison Project
JPL-M.dsf: NASA Jet Propulsion Laboratory Mascons GRACE solution, dsf refers to downscaling from 3 degree to 0.5 degree grid.
LSM: land surface model
MIPs: Model Intercomparison Projects
MODIS: Moderate Resolution Imaging Spectroradiometer
NOAH: National Center for Environmental Prediction, Oregon State University, Air Force; Hydrology Lab. (National Weather Service)
PGMD: Princeton Global Meteorological Forcing Dataset
PILPS: Project Intercomparison of Land Surface Parameterization Schemes
PCR-GLOBWB: PC Raster Global Water Balance (includes human intervention)
PCR-GLOBWB-NHI: PCR-GLOBWB with no human intervention
Q: runoff
SMAP: Soil Moisture Active Passive
SMS: soil moisture storage
STL: Seasonal Trend Decomposition using Loess
SWS: surface water storage (lakes, reservoirs, and wetlands)
VIC: Variable Infiltration Capacity model
WGHM: WaterGAP Global Hydrologic Model (includes human intervention)
WGHM-NHI: WGHM with no human intervention
WFDEI: Watch Forcing Data and ERA Interim Reanalysis

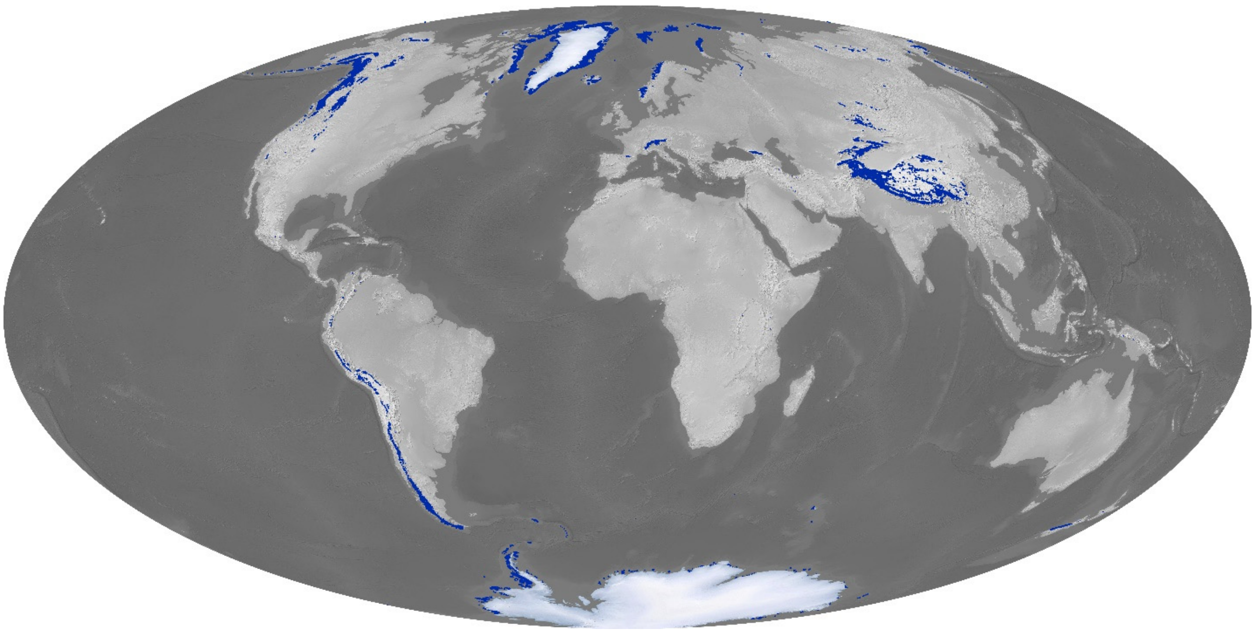

Figure S1. Global distribution of glaciers based on Randolph glacier imagery (https://eoimages.gsfc.nasa.gov/images/imagerecords/83000/83918/global_glaciers_rgi_lrg.jpg).

Section 1. Time series Decomposition and TWSA Trend Estimation

The Seasonal Trend decomposition using Loess (STL) was used to decompose TWSA monthly time series as follows:

$$S_{total} = S_{long\text{-}term} + S_{seasonal} + S_{residual} \qquad \text{(S1)}$$

where the original signal (S_{total}) is decomposed into long-term, seasonal, and residual components, based on procedures outlined in previous studies (1, 2). The long-term signal is further decomposed into linear and non-linear (interannual) components by fitting a trend using least squares linear regression and attributing the remaining long-term signal to interannual signal. The residuals reflect subseasonal signal and noise. Therefore, the TWSA trends in this study refer to the linear trends estimated from the long-term signal after STL analysis.

Previous analysis of GRACE solutions used harmonic analysis to decompose the time series (3). We compared outputs from STL and harmonic analysis, showing similar outputs from both; however, STL can isolate long-term trends without additional smoothing (Fig. S1).

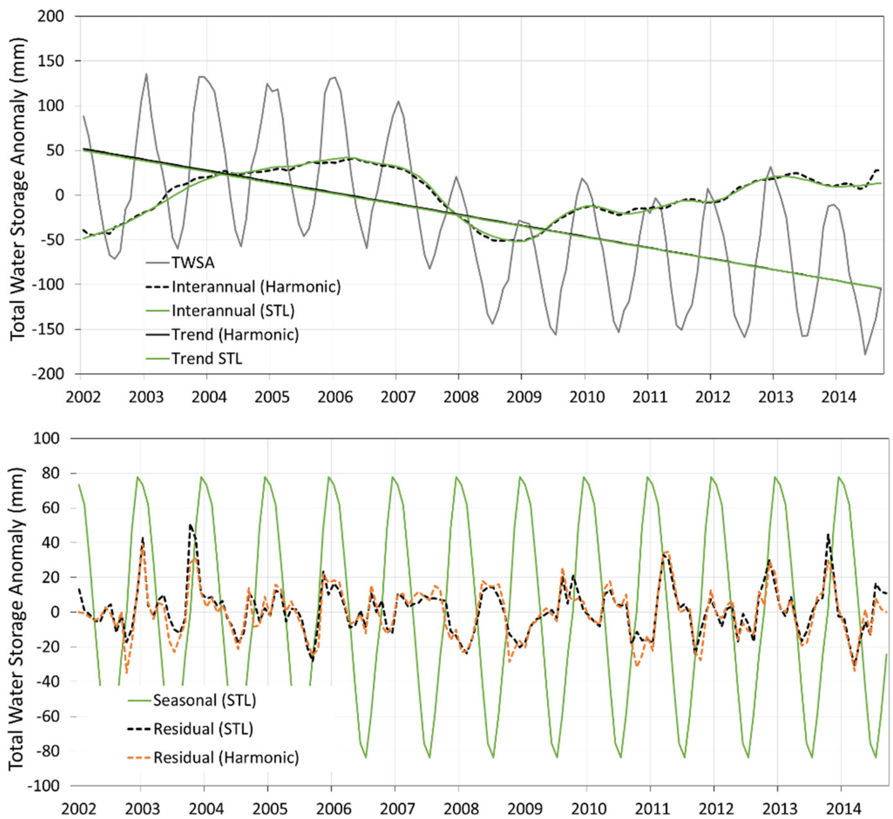

Figure S2. Comparison of TWSA time series decomposition using Seasonal Trend decomposition based on Lowess (STL) and traditional harmonic analysis for the Euphrates Basin. The upper diagram shows the raw TWSA monthly time series, the long-term trend, and the interannual fit to the data after removal of the long-term trend. The interannual fit for the harmonic analysis was based on a 13 month moving average. The lower diagram shows the seasonal fit and the residual after subtracting the long-term trend, and seasonal fits from TWSA (equation S1).

Section 2: Sources of GRACE Data

Websites for GRACE data are listed in this section.

2.1 GRACE Data

The CSR mascons GRACE TWS anomalies are described in Save et al. (2016) (4) and the data are available at http://www.csr.utexas.edu/grace/RL05_mascons.html. These data are provided at 1 degree resolution and resampled at 0.5 degrees.

Gridded spherical harmonic (GSH) data for Center for Space Research (CSR-GSHT) were obtained from the Tellus website: http://grace.jpl.nasa.gov/data/get-data/monthly-mass-grids-land/.

JPL mascons data were obtained from the Tellus website http://grace.jpl.nasa.gov/data/get-data/jpl_global_mascons/. JPL-M data are release 5 (RL05) version 2 and are described in recent papers (5-7). The 3×3 degree data are downscaled to 1×1 degree using the CLM4 model and resampled at 0.5 degrees.

Section 3. Model Descriptions

3.1 Global Hydrological Water Resource Models and Land Surface Models

Recent reviews describe many of the basic features of GHWRMs and LSMs (8-10). Global hydrological water resource models (GHWRMs) are mainly based on water balance calculations and account for human interventions, including water use and reservoir management. The two main GHWRMs evaluated in this study are PCR-GLOBWB(11) and WGHM(12). Water storage compartments in GHWRMs include snow, canopy, surface water, soil moisture, and groundwater. Surface water is routed in these models. The land surface models (LSMs) examined in this study are those included in the Global Land Data Assimilation System (GLDAS-1): Noah version (v) 2.7 (13)(13)(13)(13)(13)(13)(13)(13), Mosaic (14, 15)(14, 15)(14, 15)(14, 15)(14, 15)(14, 15)(14, 15)(14, 15, 16), Variable Infiltration Capacity, (VIC, 16), and the Common Land Model, (CLM, 17) and (GLDAS-2.1) Noah v. 3.3, and Catchment Land Surface Model (CLSM v Fortuna 2.5). CLSM in GLDAS–2 replaces Mosaic in GLDAS-1. In addition, newer versions of CLM, now termed the Community Land Model, CLM-4.0 and CLM-4.5 are included in the comparisons. All of the LSMs include water storage in canopy, snow, and soil moisture. In addition, CLM4.0 and CLM4.5 includes surface water and groundwater storage and CLSM-F2.5 includes groundwater storage. LSMs are 1 dimensional and do not simulate lateral flow. GLDAS LSMs are used to integrate observational data to produce water and energy balanced, spatially and temporally continuous global fields of land surface states (e.g., soil moisture storage) and fluxes (e.g., evapotranspiration, runoff), using knowledge of relevant physical processes as simulated within sophisticated models to ensure self-consistency (18). The model descriptions are summarized in Table S2. CLSM is also described in Koster et al. (2000) (19).

The spatial resolution of the GHWRMs is 0.5˚ (55 km at Equator) whereas that for the LSMs is 1˚ (110 km at the equator. The model time steps vary from daily for GHWRMs and aggregated to monthly outputs and 3 hr for LSMs, also aggregated to provide monthly output. GHWRM data are available from early to late 1950s to 2014 whereas LSM output are available from 1979 to present. Most of the models include some type of subgrid variability. Subgrid variability in PCR-GLOBWB includes different soil types, vegetation types (natural vegetation and rainfed and irrigated vegetation, including both short and tall types) and open water bodies (lakes, reservoirs, floodplains and reservoirs). WGHM includes 16 land cover types and open water bodies also. The GLDAS LSMs generally include subgrid variability with vegetation tiles/grid cells but do not include water bodies, such as rivers, reservoirs, and wetlands. The LSMs include a detailed soil vegetation atmosphere transfer scheme for simulating vegetation but do not include irrigated crops. The models differ in the number, thickness, and depth of the soil zone (Table S2a). Soils data for PCR-GLOBWB are derived from FAO Digital Soil Map of the World (http://www.fao.org/nr/land/soils/digital -soil-map-of-the-world). Soils data used for GLDAS LSMs are originally derived from the FAO data. GHWRMs simulate irrigation and groundwater whereas most LSMs do not, with the exception of CLM-4.0 and CLSM-F2.5, which include groundwater. Precipitation forcing for the versions of the two GHWRMs used in this study is the same and is based on Watch Forcing Data and Era Interim Reanalysis (20). GLDAS uses different forcing sources for different versions (i.e. GLDAS-1, GLDAS-2), while the LSMs in each GLDAS version are forced with the same forcing datasets (e.g. Noah and CLSM in GLDAS-2.1). The GHWRMs do not have a true energy balance built into the model framework but simulate potential ET using Penman Monteith or Priestley Taylor (Table 2a). In contrast, the LSMs have a built in detailed energy budget in their models. Runoff is simulated as saturation excess or infiltration excess flow. The GHWRMs include surface runoff, interflow (PCR-GLOBWB) and groundwater discharge to streams whereas most LSMs do not include the deeper components, except CLM-4.0 and CLSM-F2.5. Surface water is routed in the GHWRMs but not in the LSMs. The GHWRMs are mostly based on application of a daily water budget whereas the LSMs include detailed soil physics and simulate unsaturated flow based on the Richards' equation. While PCR-GLOBWB is not calibrated, WGHM is calibrated against mean annual river discharge at 1319 gauging stations by adjusting one to three parameters in the upstream cells. None of the LSMs is calibrated. One of the big differences between GHWRMs and LSMs is modeling of human intervention, including human water use and reservoir management in GHWRMs and not in LSMs. The evolution and some unique aspects of the models are described below.

The original version of WGHM greatly overestimated depletion in the Hai River Basin (-56 km^3/yr relative to GRACE CSR-M -1.2 km^3/yr, Fig. 5). Most of the Hai Basin is not calibrated to discharge in WGHM; therefore, the regionalized uncalibrated value of gamma was used (1.0). To improve the agreement with the GRACE TWSA trend, gamma was reduced from 1.0 to 0.1 and the resultant TWSA trend changed from -56 km^3/yr to -4.1 km^3/yr.

All of the models considered conserve mass. Although the term GLDAS implies data assimilation, no data assimilation is used in the LSMs included in this study.

3.2 Global Hydrological Water Resource Models

PCR-GLOBWB: PCR-GLOBWB (21, 22) is a conceptual, process-based water balance model that simulates the terrestrial hydrologic cycle, excluding Antarctica. For each grid cell (0.5°×0.5° globally) and time step (daily) it simulates the water storage in two vertically stacked soil layers and an underlying groundwater layer. The model spin-up period is 1901 – 2014 to minimize the impacts of initial conditions. Simulation of vegetation considers Leaf area index values at dormancy and at the peak of the growing cycle. Irrigated areas are based on the MIRCA2000 data set (23) combined with crop factors and growing season lengths from the global crop water model (GCWM) (24). Water use includes irrigation, industrial, domestic, and livestock sectors. Industrial and domestic water demands are based on population statistics and socioeconomic drivers (e.g., GDP and electricity production) from FAOSTAT, the UNEP (http://www.unep.org), and the World Bank (http://www.worldbank). Livestock water demand is based on Statistics of livestock densities (FAOSTAT, http://faostat.org/). Non-irrigation water demand (industry, households, and livestock) includes gross water demand and net water demand. In the case of livestock, the two demands match, for the other two sectors the difference determines the return flow which is discharged to the surface water. Non-irrigation water demand varies over time. Trends are prescribed on an annual basis as a function of population, electricity demand, and GDP per capita. In addition, domestic water demand exhibits a seasonal variation on the basis of temperature.

Irrigation water demand is computed using the FAO guidelines; irrigation is applied whenever soil moisture falls below a pre-set level and then the soil column is replenished up to field capacity in the case of non-paddy irrigation and to a water depth of 5 cm above the surface in the case of paddy irrigation. The irrigation amount is augmented to account for limited efficiency. By default, PCR-GLOBWB considers conveyance efficiency only (i.e., the irrigation water demand is increased by 40% to obtain the total irrigation water demand).

Irrigation water demand is dependent on the crop composition and the irrigated area. The crop composition does not change over time, paddy comprising wet rice, all other crops being covered by non-paddy irrigation (based on MIRCA). In these runs the fraction between paddy and non-paddy remains fixed but the total irrigated area changes over time per cell based on the FAO reported irrigated area, up to 2010. Any water applied for irrigation that does not transpire or evaporate is ultimately lost as additional groundwater discharge (return flow).

Water can be abstracted from three sources, surface water, groundwater (fossil and non-fossil), and desalinated water. The latter is prescribed, the other two fractions are determined as a function of the two year running mean, thus keeping track of the prevalence of local resources (25). These fractions determine on a monthly basis from which source water is abstracted. If for some reason the surface water amount is insufficient, the model falls back on groundwater to meet the resulting gap. Groundwater is first subtracted from the renewable groundwater; if renewable groundwater is not present, fossil groundwater is used. The amount of groundwater that can be extracted is capped by the groundwater pumping capacity which is based on data from the Intl. Water Management Institute (IWMI) and fossil groundwater is set initially at a maximum capacity from which water can only be extracted until it is fully depleted.

Water availability (surface water and groundwater) is pooled over zones of ~1 arc degree that are truncated by country borders, if applicable. Future plans are to change this to an extraction zone per cell or to include additional information on water supply (infrastructure). The downside of the current scheme is that a cell does not always have access to its nearest water resources as they may lie outside its prescribed abstraction zone. However, the influence of this on 30 arc seconds should be relatively minor.

The dynamic water allocation is not always in line with local preferences or infrastructure. Thus, there is a possibility to use literature fractions of groundwater use and we rely widely on existing data sets for cities (26) for irrigation (27). Whenever these data are not fully reliable (i.e., extrapolated data), preference is given to the dynamic water allocation scheme. This blend of prescribed and dynamic allocation leads to similarity between WaterGap and PCR-GLOBWB where the quality of the empirical data is strong but to increased differences and stronger dynamics in PCR-GLOBWB where the quality of the data is poor;

Surface water availability is defined by storage in channels, lakes, and reservoirs within each cell and abstraction zone. This storage is modified by reservoir operations in the upstream area. Currently reservoir outflow is a function of reservoir storage only. Future model development will include downstream water demand to determine reservoir operations.

- URL: http://www.globalhydrology.nl/models/PCR-GLOBWB-2-0/

WGHM 2.2(a): Water GAP(28) consists of both the WaterGAP Global Hydrological Model (WGHM)(12) and five water use models for the following sectors: irrigation, livestock, household, manufacturing, and cooling of thermal power plants. The model spin-up period is 1901 – 2014 to minimize the impacts of initial conditions. Water use is modeled by computing water withdrawals and consumptive water uses in each grid cell. Consumptive irrigation water use is computed by the Global Irrigation Model (GIM) as a function of irrigated area (27, 28(29)(29)(29)(29)(29)(29)(29), 29) and climate in each grid cell. Taking into account information on the source of water, and making assumptions on irrigation water use efficiencies and return flows, the sub-model GWSWUSE (Ground Water Surface Water Use) computes net abstractions from groundwater (NA_g) and from surface water (NA_s)(30). Regarding crops, only rice and non-rice crops are distinguished, and crop growth periods are not prescribed but modeled. Water withdrawals are calculated by dividing consumptive use by a country-specific irrigation water use efficiency. Livestock water use is calculated as a function of the animal numbers and water requirements of different livestock types. Grid cell values of domestic and manufacturing water use are based on national values that are downscaled to the grid cells using population density. Power plant cooling water use takes into account the location of more than 60,000 power plants, their cooling type, and their electricity production.

WGHM computes time series of fast-surface and subsurface runoff, groundwater recharge, and river discharge, as well as storage variations of water in canopy, snow, surface water, soil, groundwater, lakes, man-made reservoirs, wetlands and rivers as a function of climate, soil, land cover, relief and observed river discharge. Location and size of lakes, reservoirs and wetlands are defined by the global lakes and wetland database (GLWD), with an addition of more than 6000 man-made reservoirs (12). Groundwater storage is affected by diffuse groundwater recharge via the soil, which is modeled as a function of total runoff, relief, soil texture, hydrogeology, and the existence of permafrost or glaciers. Focused groundwater recharge from rivers, lakes, and wetlands is taken into account in WGHM in semi-arid and arid regions in a simple manner.

Water abstractions are derived from surface water or groundwater during pre-processing. Therefore, WGHM does not dynamically allocate water. Groundwater use during a model run is not dependent on surface water availability. WGHM has unlimited groundwater availability and does not distinguish between renewable and nonrenewable groundwater. For abstractions from surface water, the sequence is: 1) global lakes, 2) reservoirs, 3) river, and 4) local lakes according to water availability. Water use can be satisfied up to one year after demand. Irrigation water demand is climate-dependent but non-irrigation water uses are not climate-dependent. Deficit irrigation (70% of full irrigation demand) is modeled in semiarid regions with substantial amounts of irrigation as well as ongoing groundwater depletion. Water demand for irrigation varies annually based on time varying irrigated area from FAO. Non-irrigation water demand varies over time. Trends are prescribed on an annual basis as a function of population, electricity demand, and GDP per capita. In addition, domestic water demand varies seasonally on the basis of temperature. Current research on WGHM includes addition of a gradient-based groundwater model and a glacier model.

- URL:http://www.uni-Frankfurt.de/fb/fb11/ipg/ag/dl/datensaetze/1_irrigation_map/index.html

3.3 Land Surface Models (LSMs)

The LSMs considered in this study include models from the Global Land Data Assimilation System (GLDAS) version 1 and 2.1 and newer versions of the Community Land Model (version 4.0).

Global Land Data Assimilation System: A Global Land Data Assimilation System (GLDAS) is a global, high-resolution, offline (uncoupled from the atmosphere) modeling system that incorporates satellite- and ground-based observations to produce optimal fields of land surface states and fluxes in near-real time for predicting response of water resources to climate variability (18). GLDAS was developed jointly by NASA Goddard Space Flight Center (GSFC) and National Oceanic and Atmospheric Administration (NOAA) National Center for Environmental Prediction (NCEP).

GLDAS makes use of the new generation of ground- and space-based observation systems, which provide data to constrain the modeled land surface states. Constraints are applied in two ways: (1) by forcing the LSMs with observation-based meteorological fields, biases in atmospheric model-based forcing can be reduced, and (2) by employing data assimilation techniques, observations of land surface states can be used to curb unrealistic model states.

GLDAS Version 1 products (GLDAS-1) include four LSM outputs from NOAH version 2.7, Mosaic, VIC, and CLM version 2.0 at 1 degree resolution, extending from 1979 to present. The simulations were derived with the same forcing datasets, used a common set of land surface characteristics datasets, and were initialized in the same manner. **GLDAS-1** LSMs are forced with different sources over time, including ECMWF data from 1979 – 1993; NCAR reanalysis from 1994 – 1999; NOAA/GDAS for 2000 and with the period since 2001 forced with NOAA/Global Data Assimilation System (GDAS) atmospheric analysis fields (31), the Air Force Weather Agency's AGRicultural METeorological modeling system (AGRMET) radiation fields, and NOAA Climate Prediction Center Merged Analysis of Precipitation (CMAP) fields (32). The spin-up for GLDAS-1 models (MOSAIC and VIC) is based on initializing with the climatological state for Jan 1, 1979. The climatological state is derived from the average of the 1979 – 1989 run. Previous comparisons of different initializations and spin-ups found that this approach was optimal (33). GLDAS-1 LSMs simulate subgrid variability based on 1-13 vegetation tiles per grid cell, using a static, 1-km resolution, land cover classification from the University of Maryland (UMD) based on the Advanced Very High Resolution Radar (AVHRR) observations. Vegetation type is linked to albedo and roughness height. GLDAS-1 also ingests a satellite-based, 1-km resolution climatology of Leaf Area Index (LAI). The soil texture class for respective models is assigned based on percentages of sand, silt, and clay in a given grid cell, using a global soils dataset (5´) (34).

GLDAS Version 2 products (GLDAS-2) currently include two LSM outputs from Noah version 3.3 and CLSM version Fortuna 2.5 (CLSM-F2.5), and are forced entirely with the Princeton Global Meteorological Forcing Dataset (35) from 1948-2010. The spin-up for GLDAS-2 models is based on initializing with the climatological state for Jan 1, 1948. The climatological state is derived from the average of the last 10 years of the 1948 – 1959 run. Previous comparisons of different initializations and spin-ups found that this approach was optimal (33).A branch off simulation starts in 2001, forced with GDAS atmospheric analysis fields, AGRMET radiation fields, and the Global Precipitation Climatology Project (GPCP)(36) (hereafter, GLDAS-2.1). GLDAS-2.1 addressed unnatural trends and uncertain forcing fields observed in GLDAS-1, upgraded LSMs version, and included other enhancements related to initialization and surface datasets. In contrast to GLDAS-1, GLDAS-2 LSMs use respective model default parameters and settings, and switched to MODIS-based land surface datasets.

URL: http://disc.sci.gsfc.nasa.gov/hydrology/data-holdings

NOAH in GLDAS-1 and GLDAS-2:

The NOAH model (37, 38) has been used operationally in the National Center for Environmental Prediction models since 1996 and is continually improved. The version of Noah used in GLDAS-1 is 2.7, while that in GLDAS-2 is 3.3. Inherited from the Oregon State University model, the land surface scheme has an explicit vegetation canopy, soil hydrology, and soil thermodynamics. The scheme is moderate complexity with single unified ground/vegetation surface (i.e. one surface temperature). The model includes four soil layers (2 m deep), single layer snowpack, and frozen soil physics. Both versions of NOAH only include canopy, snow, and soil moisture storage.

MOSAIC in GLDAS-1: Mosaic (39) LSM was originally developed for the fully coupled system in the General Circulation Model at NASA/GSFC. A unique aspect of MOSAIC is its treatment of subgrid-scale variability, dividing each model grid cell into a mosaic of tiles(40) based on the distribution of vegetation types within the cell. The vegetation tiling approach was adopted to all GLDAS LSMs where multiple type and/or bare soil can coexist within a grid if they cover more than 10% of total tiles. Surface flux calculations are similar to those described by Sellers et al. (41). The model includes a canopy interception reservoir, a single-layer snowpack, and three soil layers. Many of the model attributes are similar to those of NOAH (Table S2a).

VIC in GLDAS-1: Variable Infiltration Capacity (VIC) was developed by Liang et al. (16) and is continuously evolving at University of Washington. The infiltration and surface runoff scheme are based on Xianjiang model (42), in which the conceptual schemes are used to represent the surface runoff and base flow. The subgrid heterogeneity in land cover, topography, and precipitation are modeled by a mosaic-type representation. As a macroscale hydrological model, VIC models subgrid variability in the soil moisture storage capacity and base flow as a nonlinear recession. The version used in GLDAS-1 is 4.0.4 which includes three soil layers (43) and was simulated in water balance mode with an energy balance and without the frozen soil algorithm (44). Canopy water storage and lake water storage are not included in this version of the model. In the water balance mode, the soil surface temperature is assumed to be the air temperature for the current time step, eliminating the ground heat flux solution and the interactive processes required to close the surface energy balance.

CLM-2.0 in GLDAS-1: Community Land Model (CLM, (45)) was developed by a collaboration of scientists with interests in making a general land surface model available for public use at the National Center for Atmospheric Research (NCAR). CLM2.0 includes superior components from each of three contributing models: the NCAR LSM (46), the Biosphere-Atmosphere Transfer Scheme, and the LSM of the Institute of Atmospheric Physics of the Chinese Academy of Sciences (47). CLM2.0 includes canopy, snow, and soil moisture storage compartments. CLM has added complexity including ten soil layers, multiple snow layers, and one vegetation layer. The subgrid variability is represented as the plant functional type (PFT) and bare ground, instead of a land cover class. The Plant Functional Types (PFT) capture the biophysical and biochemical differences between plants as to their functional characteristics. The version of CLM in GLDAS-1 is admittedly older, 2.0.

CLM-4.0: Details of the newer versions of CLM are provided in Technical Notes (48, 49). Surface water is routed using a simplified version of the TOPModel (50) and groundwater storage is modeled using a simplified unconfined groundwater scheme (51). In this study, CLM4.0 simulations were forced with atmospheric data for the period 1900 – 2014 from the CRU-NCEP data set (52).

CLSM-F2.5 in GLDAS-2.1

The Catchment Land Surface Model (CLSM (19)) was developed as a new strategy for improved characterization of subgrid soil moisture variability and its impact on runoff and evaporation generation. The version of CLSM used in this study is Fortuna 2.5 within GLDAS 2.1. The CLSM uses topographically derived catchment as the land surface element, instead of a grid in traditional LSMs. Subcatchment variability of soil moisture is dynamically distributed into fractions of saturated, not saturated, and below wilting point, each regime controlled by appropriate runoff and evaporation processes. Unlike other LSMs, CLSM doesn't have vertical soil layers. The primary soil moisture prognostic variable is the catchment deficit, defined as the average amount of water that would have to be added to bring the catchment to saturation. The vertical distribution of equilibrium soil moisture profile is derived from the relations of Clapp and Hornberger (1978) (53). CLSM does not explicitly model the water table depth but water table depth is estimated by using the TOPMODEL formulation (54) for the topographic index. The energy balance calculations and canopy interception reservoir formulation are exactly as in the Mosaic model. Snow is represented with the three-layer snow model (55). In addition to canopy, snow, and soil moisture, groundwater storage can be estimated from the catchment deficit and the maximum water capacity, based on the depth to bedrock. Previous studies have increased the bedrock depth uniformly by 2 m to capture the dynamic range in total water storage (56). CLSM is the land model in the Goddard Earth Observing System Model Version 5 (GEOS-5) system at NASA/GMAO.

Section 4.0: Uncertainty in GRACE Data

Approaches used to estimate data uncertainties related to measurement and leakage are similar to those described in Scanlon et al. (57). These descriptions are repeated in this section.

4.1 Measurement and Leakage Uncertainties

Center for Space Research Mascons

Uncertainties in CSR-M data are based on the residuals after removing the component signals (long-term trend [including interannual] and seasonal) using STL analysis (equation S1). The root mean square (RMS) of the residual is used to approximate the measurement uncertainty in CSR-M. We realize that this approach may overestimate the uncertainty because the residual may still contain sub-seasonal signal. Because of the high grid resolution of CSR-M (1˚) leakage errors were assumed to be negligible and were neglected.

Jet Propulsion Lab Mascons

Measurement and leakage errors were considered in JPL-M solutions. Measurement errors for each mascon are prescribed by the diagonal elements of the formal posteriori covariance matrix from the GRACE data inversion, scaled by a factor 2. The factor 2 is empirical, and is selected to roughly match the magnitude of the residuals with respect to a fit of a linear and annual component for each mascon (58). These residuals represent both GRACE measurement noise, as well as real interannual signal; as such, the factor 2 is assumed to provide a conservative estimate of uncertainty. Measurement errors over a basin are calculated using an area-weighted root sum of squares of measurement errors for each mascon element within the basin.

Leakage errors arise because the shape of the hydrological basins does not precisely conform to the boundaries of the mascon elements. Leakage errors are quantified through a synthetic simulation. We create a 5-year (2005-2009) monthly time series of hydrology and ocean mass variations at 1^{o} x 1^{o} spatial resolution by combining the CLM (hydrology) model (59) and the OMCT (60) (ocean) model. This composite model is then mascon-averaged to emulate the spatial sampling of the JPL mascon solution. We then apply the CRI filter to the composite model to correct for leakage error across coastlines, and apply two sets of gain factors: one derived from the CLM model, and the other from the GLDAS land surface hydrology model (18). We then compute basin averages using both the original composite model at 1^{o} x 1^{o} spatial resolution, and the model after it has been mascon-averaged, CRI-filtered, and scaled. The RMS of the monthly differences between the two time series for each basin represents the leakage error. Because we study the effects of two differing hydrology models in computing the gain factors (GLDAS and CLM), the final reported leakage error is the average between the two computed RMS values using each set of gain factors. This method of computing leakage error is similar to what is performed in a previous study (7); the reader is referred to this article for more information.

The combined measurement and leakage error is calculated by summing the individual errors in quadrature (RSS, Root Sum of Squares of measurement and leakage errors).

Because of the Kalman filter time correlation used in processing JPL-M, the gravity estimate for all previous months changes slightly with the processing of each additional month. Each time data for a new month are released, data for all previous months are updated.

Gridded Spherical Harmonics (CSR)

In the gridded GRACE SH solutions, uncertainty estimates (cm water) are provided on the Tellus website, including GRACE measurement errors and leakage errors. Measurement errors are based on the TWSA residuals after subtracting the long-term trend and annual and interannual signals. This approach may overestimate the uncertainties because the residuals may contain interannual and subseasonal signals in addition to noise. Grid cell measurement errors are multiplied by the scaling factors and are highest near the equator (up to 36 mm) and decrease towards the poles (61). This poleward trend is attributed to greater satellite ground tracks near the poles. Leakage errors are estimated from the root mean square (RMS) difference between the unfiltered and filtered (truncated and 300 km Gaussian filter) monthly mean TWS estimates from the CLM-4.0 model which are then multiplied by the ratio of RMS variability of the filtered GRACE and CLM4 time series (61):

$$E_g^L = RMS(\Delta S_T - k\Delta S_F)\,\frac{RMS_{GRACE}}{RMS_{model}} \tag{S2}$$

where the subscript g is grid cell, superscript L is leakage, ST is true water storage estimated from the CLM4 model and SF is filtered water storage from GRACE, and k is the scaling factor. The leakage error is multiplied by the ratio of the RMS of GRACE and the CLM4 model because the amplitude of the GRACE signal is generally much greater than that of the model. Leakage errors are residual errors after filtering and rescaling. Both measurement and leakage errors are considered time invariant. The total error in TWSA for each grid cell is calculated by summing the measurement and leakage errors in quadrature for each grid cell:

$$E_{tot} = \sqrt{\left(E_g^M\right)^{+2} + \left(E_g^L\right)^2} \tag{S3}$$

Basin Scale Errors

Estimated total errors in a basin are less than the average of grid cell errors because of spatial correlation (Long et al., 2015). Basin scale errors were calculated following Landerer and Swenson (2012) (61):

$$\sigma_{mb(lb)} = \sqrt{var}/N \tag{S4}$$

$$Var = \sum_{i=1}^{n}\sum_{j=1}^{n} w_i\, w_j Cov(x_i x_j) \tag{S5}$$

$$Cov\left(x_i x_j\right) = \sigma_i \sigma_j exp\left(\frac{-d_{i,j}^2}{2d_0^2}\right) \tag{S6}$$

$$d_{i,j} = a\,\frac{\pi}{180} A\sqrt{[(long(i) - long(j)\cos\left(lat(i)\right)]^2 + [lat(i) - lat(j)]^2} \tag{S7}$$

where σ_{mb} is the measurement error of a basin; σ_{lb} is the leakage error of a basin; N is number of grid cells in a basin; subscripts i and j represent two different grid cells in a basin; Var is the measurement or leakage error variance of mean TWSA of a basin; w is the area weight at each grid cell in the basin and simplified to 1/N under the assumption of equal contribution from each grid cell to the basin average TWSA; Cov is the covariance between two grid cells; σ is the standard deviation of measurement or leakage error of a grid cell; $d_{i,j}$ is the distance between two grid cells; d_0 is a decorrelation-length scale, i.e., 300 km for measurement error and 100 km for leakage error; a is the radius of the Earth (6,371 km); and long and lat denote longitude and latitude of a grid cell (62).

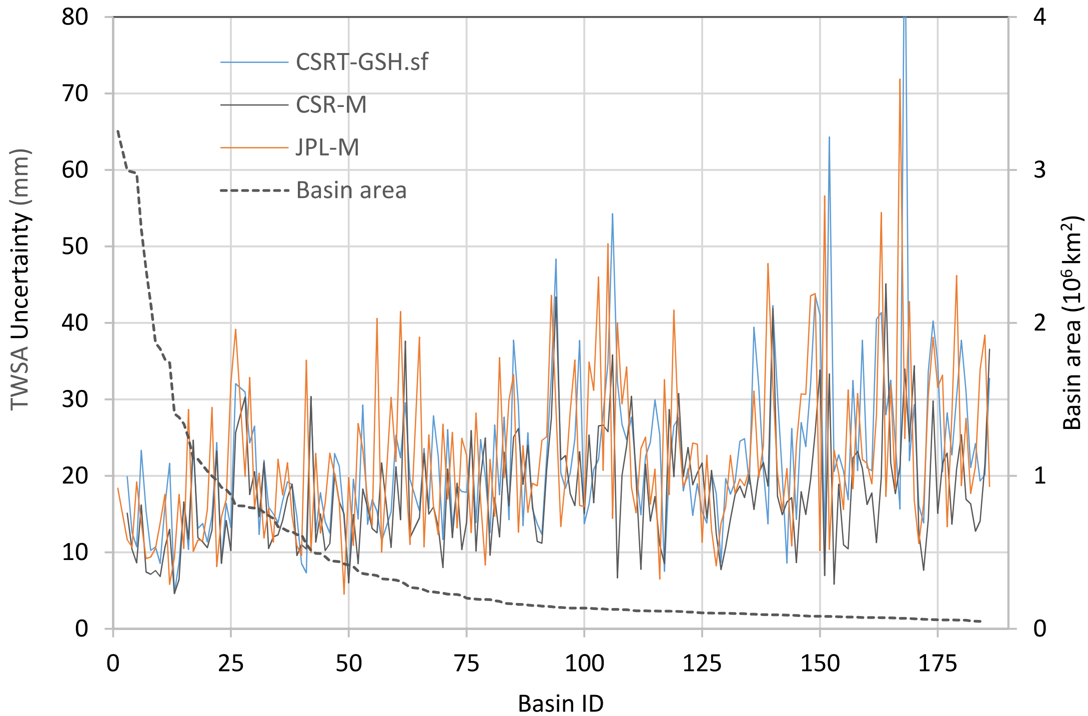

Figure S3. Uncertainty estimates calculated from residuals in equation S1 for the three GRACE solutions. These estimates of TWSA errors may overestimate actual errors because the residuals may contain subseasonal signal.

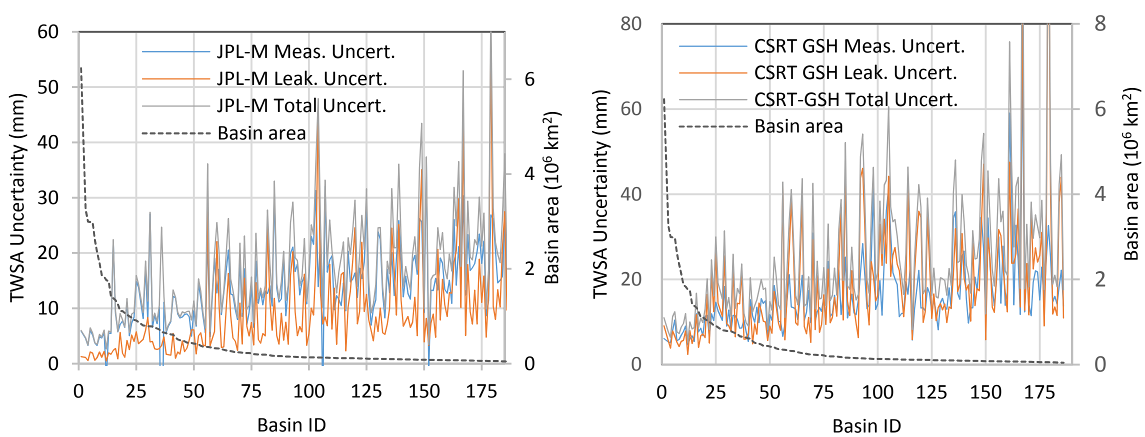

Figure S4. Uncertainty estimates for JPL-M and CSRT-GSH, including measurement, leakage, and total (sum measurement and leakage) uncertainties.

Table S1. Summary of measurement and leakage errors for the three GRACE solutions according to basin areas (large: ≥0.5x10^6 km^2; medium (0.1x10^6 to 0.5x10^6 km^2; small, ≤0.1x10^6 km^2). The total error is estimated by summing the measurement and leakage errors in quadrature. RMS is root mean square. RMS of residuals assumes the residuals from the time decomposition (equation 1) approximates the error.

Error (mm)	*CSRT-GSH*			*JPL-M(v2)*			*RMS of residuals (STL analysis)*		
Area	*Measure-ment*	*Leakage*	*Total Error*	*Measure-ment*	*Leakage*	*Total Error*	*CSRT-GSH.sf*	*CSR-M*	*JPL-M.sf*
Median Error (mm)									
≥0.5 x10^6 km^2	8.6	7.9	12.0	6.8	2.4	7.7	15.0	12.0	14.7
0.1 < Area <0.5	13.5	15.0	20.7	13.1	6.8	15.7	20.0	17.7	20.7
≤0.1 x10^6 km^2	19.7	23.3	31.9	16.5	10.5	20.8	26.6	18.3	24.0
Mean Error (mm)									
≥0.5 x10^6 km^2	9.1	10.0	13.8	7.4	2.8	9.3	16.3	13.9	16.7
0.1 < area <0.5	15.9	18.7	25.2	14.1	9.1	17.5	21.1	18.3	22.1
≤0.1 x10^6 km^2	22.4	26.3	35.3	17.6	14.2	23.3	28.6	20.0	27.4

4.2 Uncertainties in GRACE TWSA Trends

The uncertainties in GRACE TWSA trends incorporates

(1) variability among the three GRACE solutions (solution uncertainty),

(2) uncertainty in the trend (slope of linear regression) for each solution based on linear regression, and

(3) uncertainty related to glacial isostatic adjustment (GIA)

To estimate solution uncertainty we calculated the standard deviation of the trends from the three GRACE solutions. Trend uncertainties reflect uncertainties in the slopes from the linear regression analysis for each solution and then the standard deviation of the three trend uncertainties was calculated. Uncertainties related to GIA were computed from the 1-sigma model ensemble differences from four different global GIA models, including the new ICE-6G model (63), and three other models (64-66).

Uncertainties from all three sources were combined by summing the uncertainties in quadrature (RSS, root sum of squares).

Net TWSA trends were estimated by summing trends over all basins. The corresponding uncertainty was estimated by summing the combined uncertainties for each basin in quadrature (RSS).

4.2a Uncertainty in Contribution of Land Water Storage to Global Mean Sea Level

Geocenter corrections impact TWSA trends because there are more continents in the northern hemisphere and these corrections are incorporated into each GRACE solution. However, there are uncertainties in these corrections, which are described in Reager et al. (67). We apply the uncertainty of 0.05 mm/yr from this source in our estimate of uncertainty in the land water storage contribution to GMSL along with the 0.04 mm/yr uncertainty from GRACE solutions, trends, and GIA, resulting in a total uncertainty of 0.09 mm/yr (Fig. 7).

4.2b Testing Significance of TWSA Trends

To assess the significance of the trends we performed the Mann-Kendall test on the long-term TWSA data based on the STL analysis (equation 1, data after removal of seasonal and residuals). Because our analysis focused on basin scale TWSA rather than grid scale TWSA as in the previous study, problems with leakage and spatial correlation should be greatly reduced with basin scale mascons. We focused the analysis on basins with large decreasing or increasing trends (trends outside ±0.5 km^3/yr). Results show that all basins show significant trends in at least one of the three GRACE solutions (CSR-M, JPL-M.dsf, and CSRT-GSH.sf) with the exception of the Congo basin where none of the solutions was significant. Approximately 85% of the basins have significant trends in all three GRACE soltuions and ~15% of the basins had significant trends in at least 2 GRACE solutions.

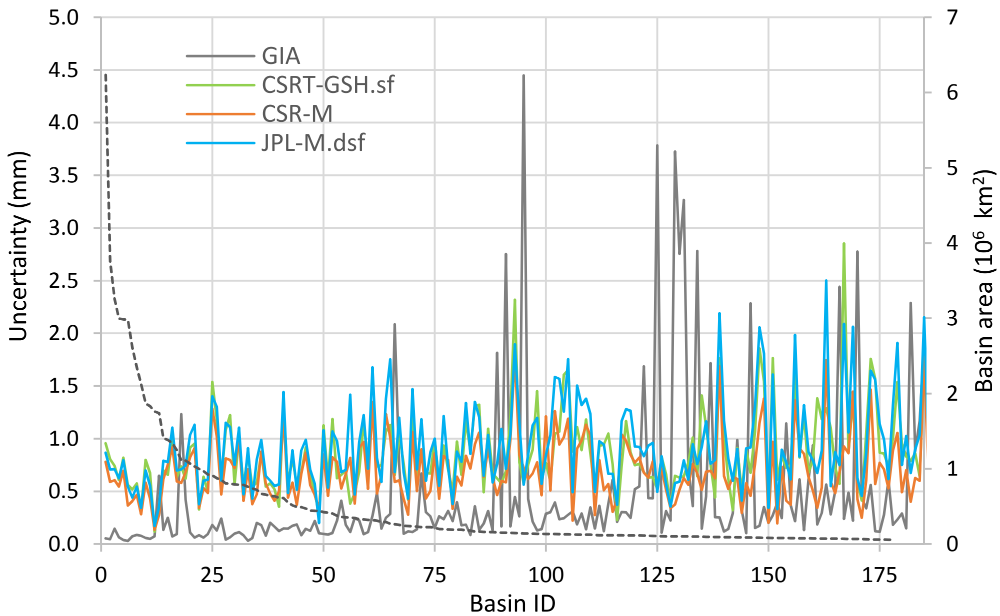

Figure S5. Uncertainties in TWSA trends for GRACE CSR-M, JPL-M and CSRT-GSH.sf solutions for the 186 basins, ranked according to basin area. Uncertainties related to glacial isostatic adjustment are also shown based on averaging uncertainties for 4 models.

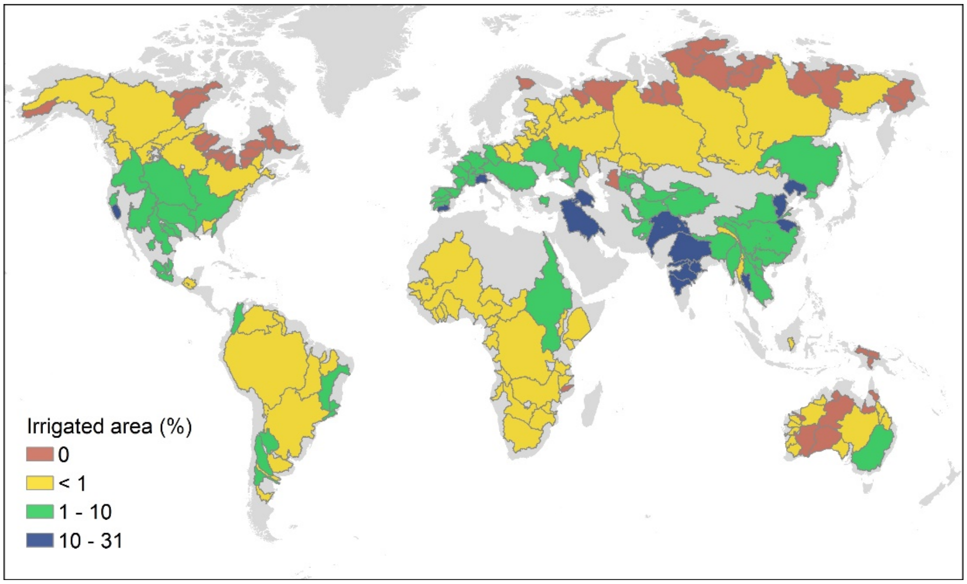

Figure S6. Percent irrigation in river basins examined in this study based on data from Food and Agricultural Organization (FAO) Global Map of Irrigated Areas (http://www.fao.org/nr/water/aquastat/irrigationmap/index.stm).

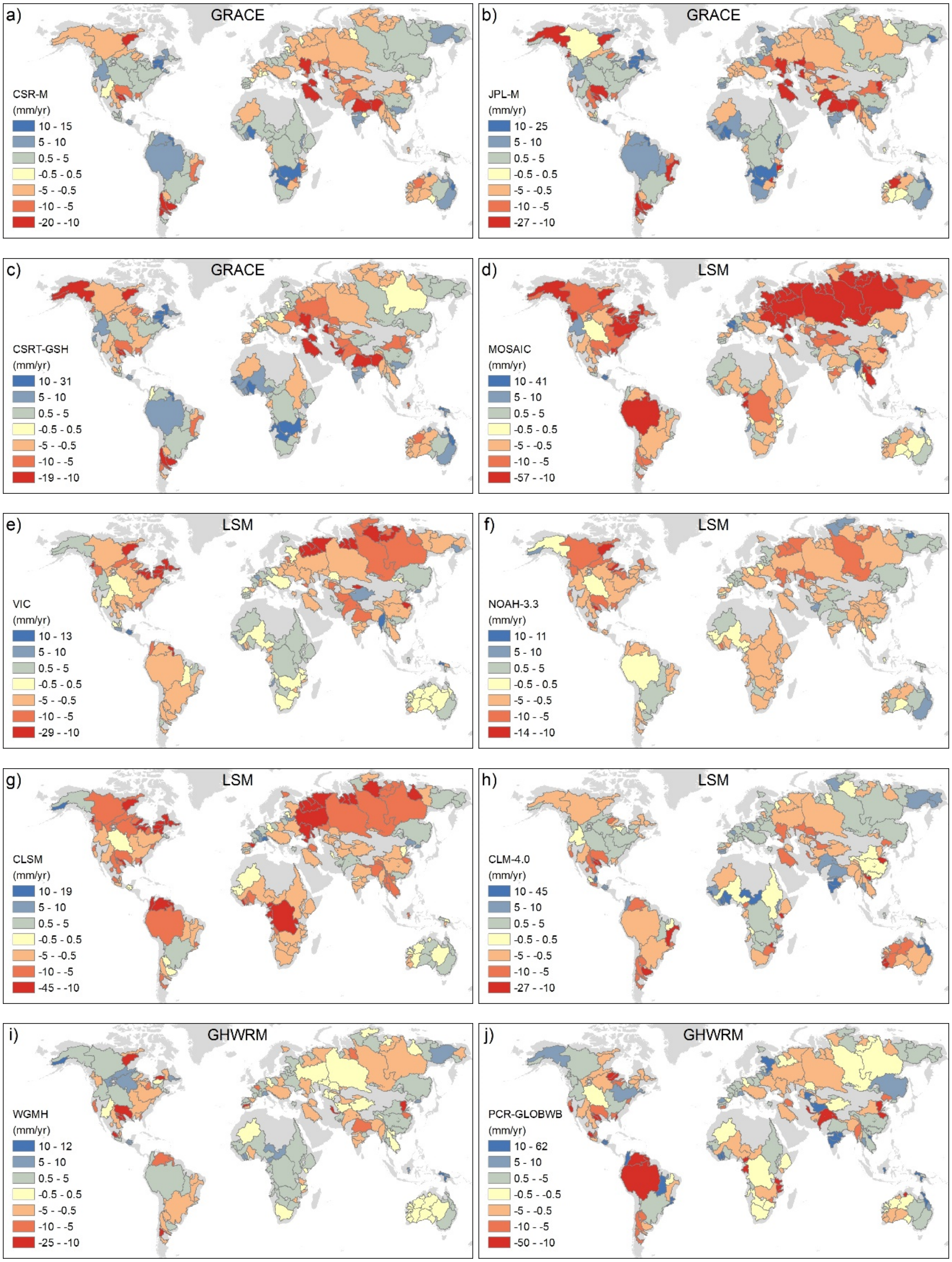

Figure S7. Long-term (Apr. 2002 – Dec 2014) trends in total water storage anomalies (anomalies based on 2004 – 2009) expressed in **mm/yr** from GRACE ([a] CSR-M, [b] JPL-M, and [c] CSRT-GSH), land surface models (d) MOSAIC and (e) VIC from GLDAS-1.0 and (f) NOAH-3.3 and (g) CLSM-F2.5 from GLDAS-2.1 and (f) and GHWRMs, including (i) WGHM and (j) PCR-GLOBCLM-4.0).

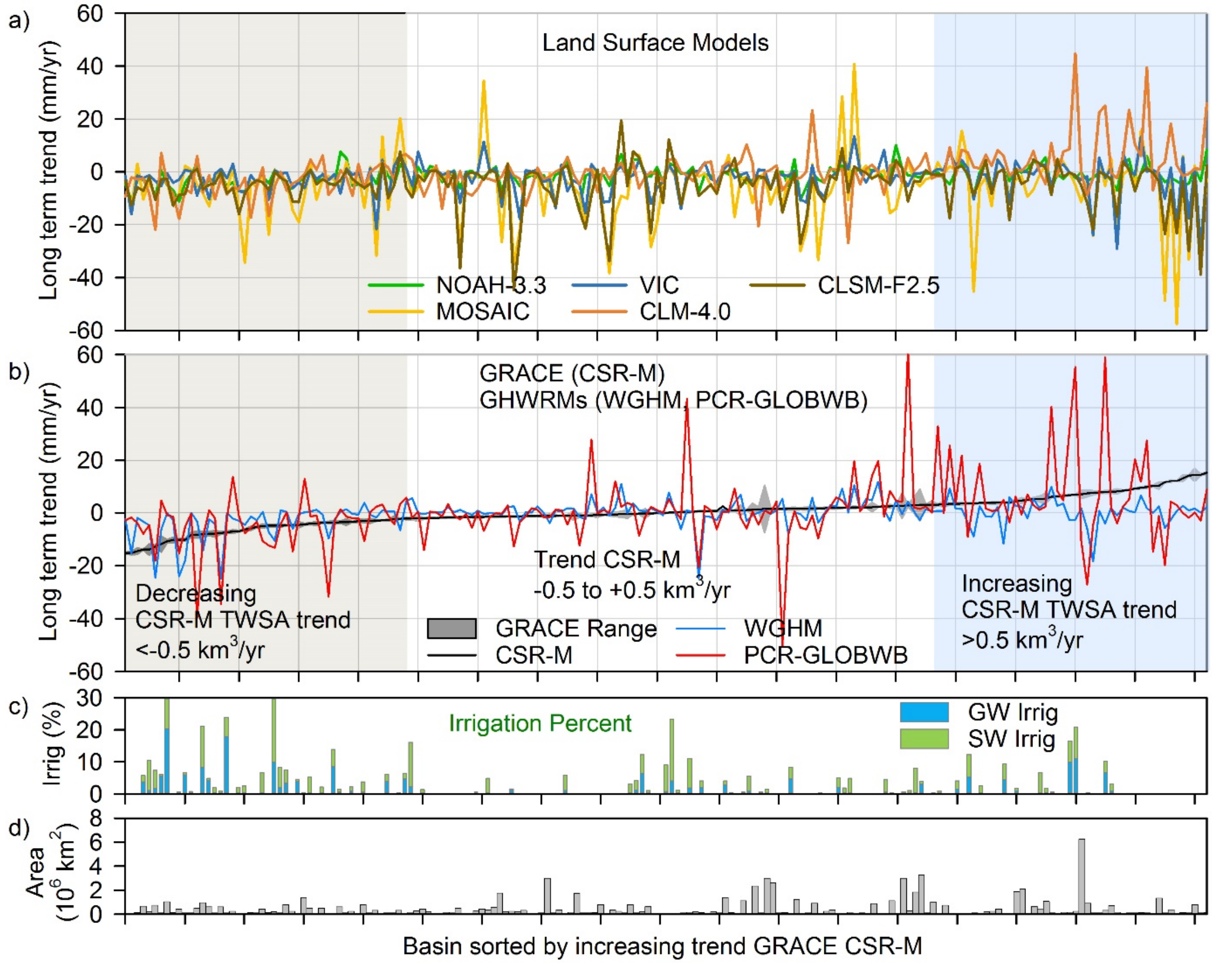

Figure S8. TWSA trends ranked according to trends from GRACE CSR-M from decreasing trends (buff background, ≤-0.5 km^3/yr) and increasing trends (blue, ≥0.5 km^3/yr). Gray shaded area shows range from three GRACE solutions (b). Trends from LSMs (NOAH-3.3, MOSAIC, VIC, CLM-4.0, and CLSM-F2.5) are shown in (a) and trends from GHWRMs (WGHM; PCR-GLOBWB) are shown in (b). Percent irrigated area of basins is shown in (c) with groundwater based irrigation in blue and surface water based irrigation in green.

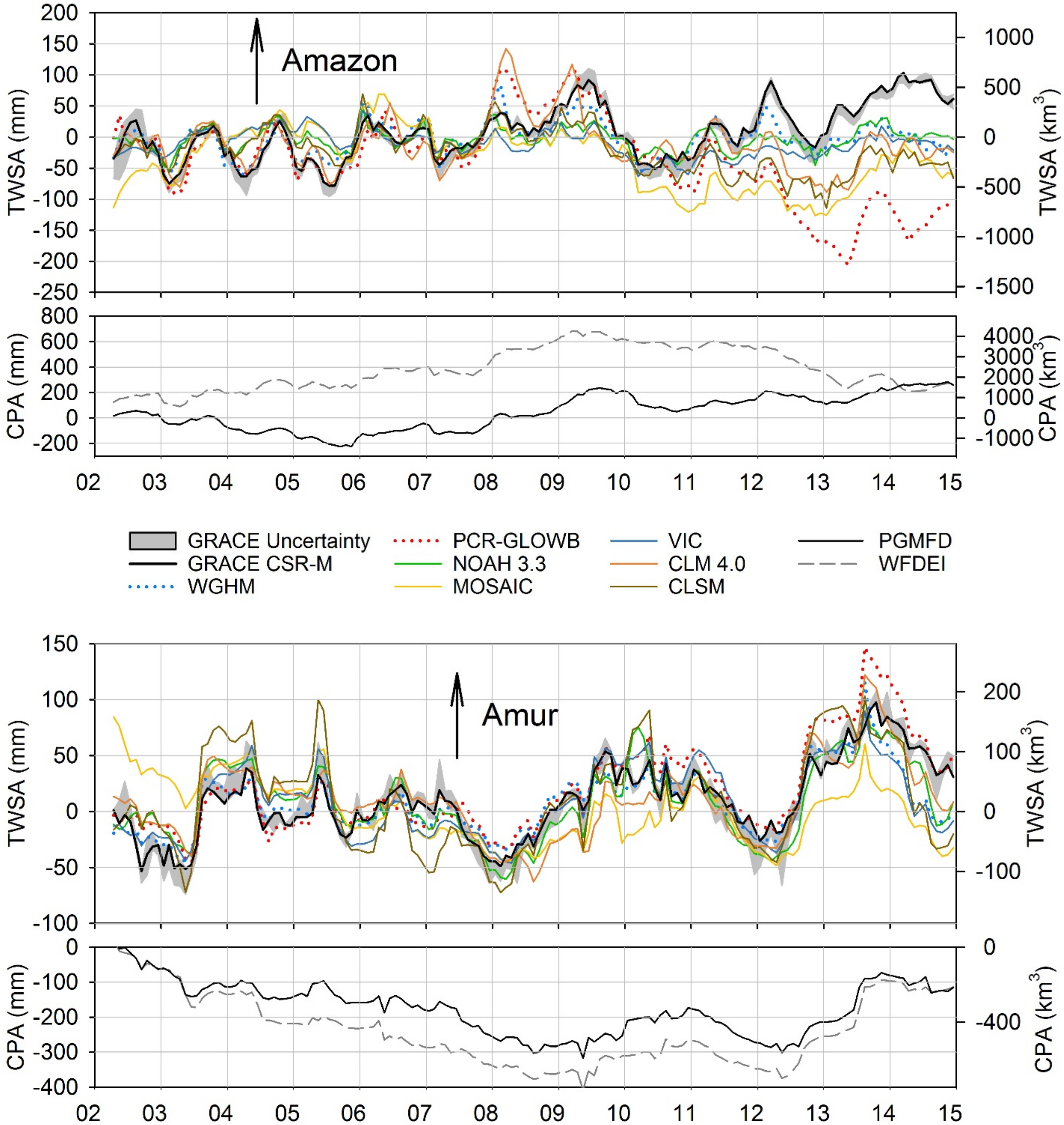

Figure S9. Time series of Total Water Storage Anomalies (TWSA) (deseasonalized) for Amazon and Amur basins and cumulative precipitation anomaly from Princeton Global Meteorological Forcing Dataset (PGMFD) from NOAH-3.3 (GLDAS-2.1) and WFDEI.

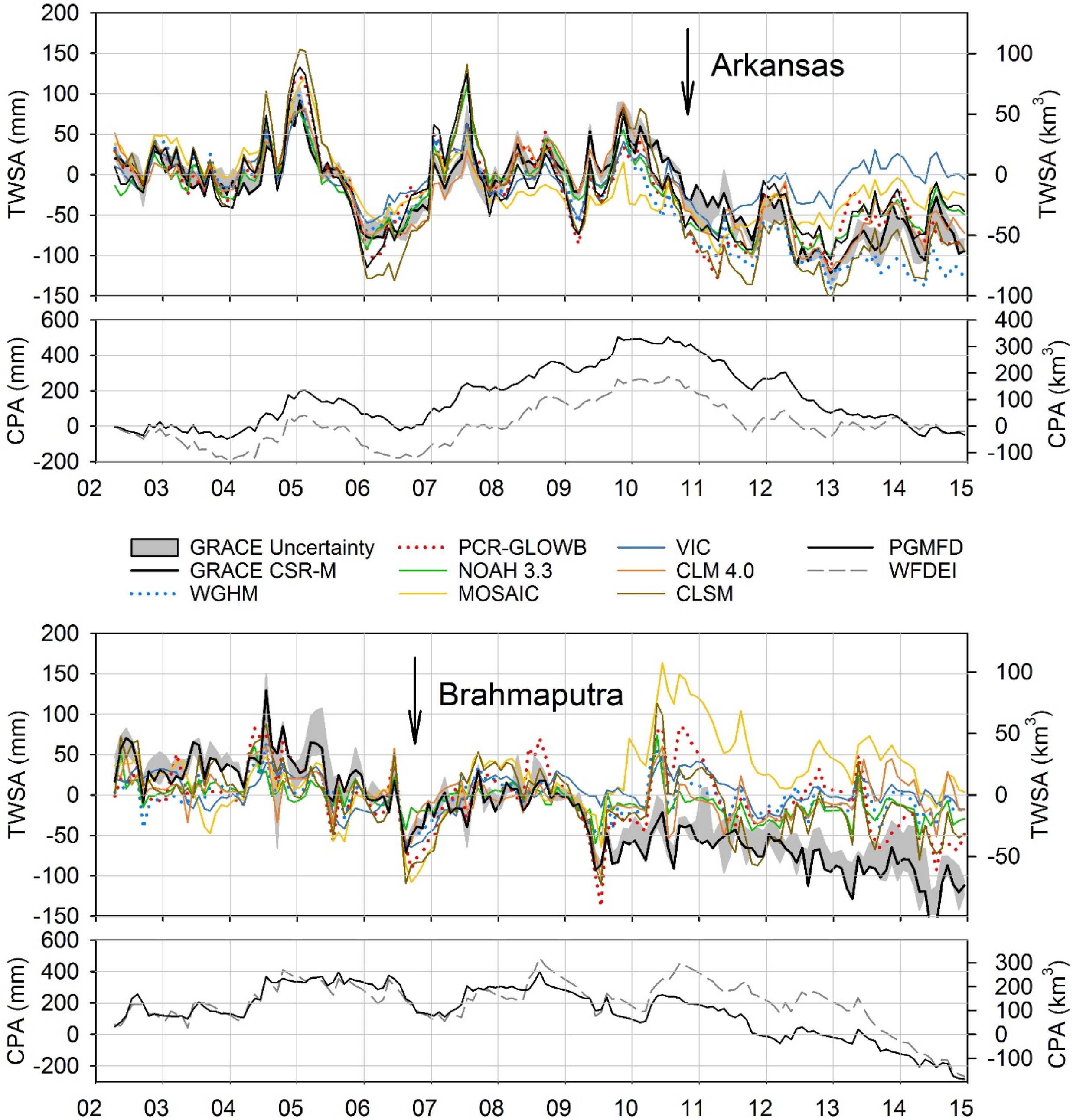

Figure S9 (cted.). Time series of Total Water Storage Anomalies (TWSA) (deseasonalized) for Arkansas and Brahmaputra basins and cumulative precipitation anomaly Princeton Global Meteorological Forcing Dataset (PGMFD) from NOAH-3.3 (GLDAS-2.1) and WFDEI.

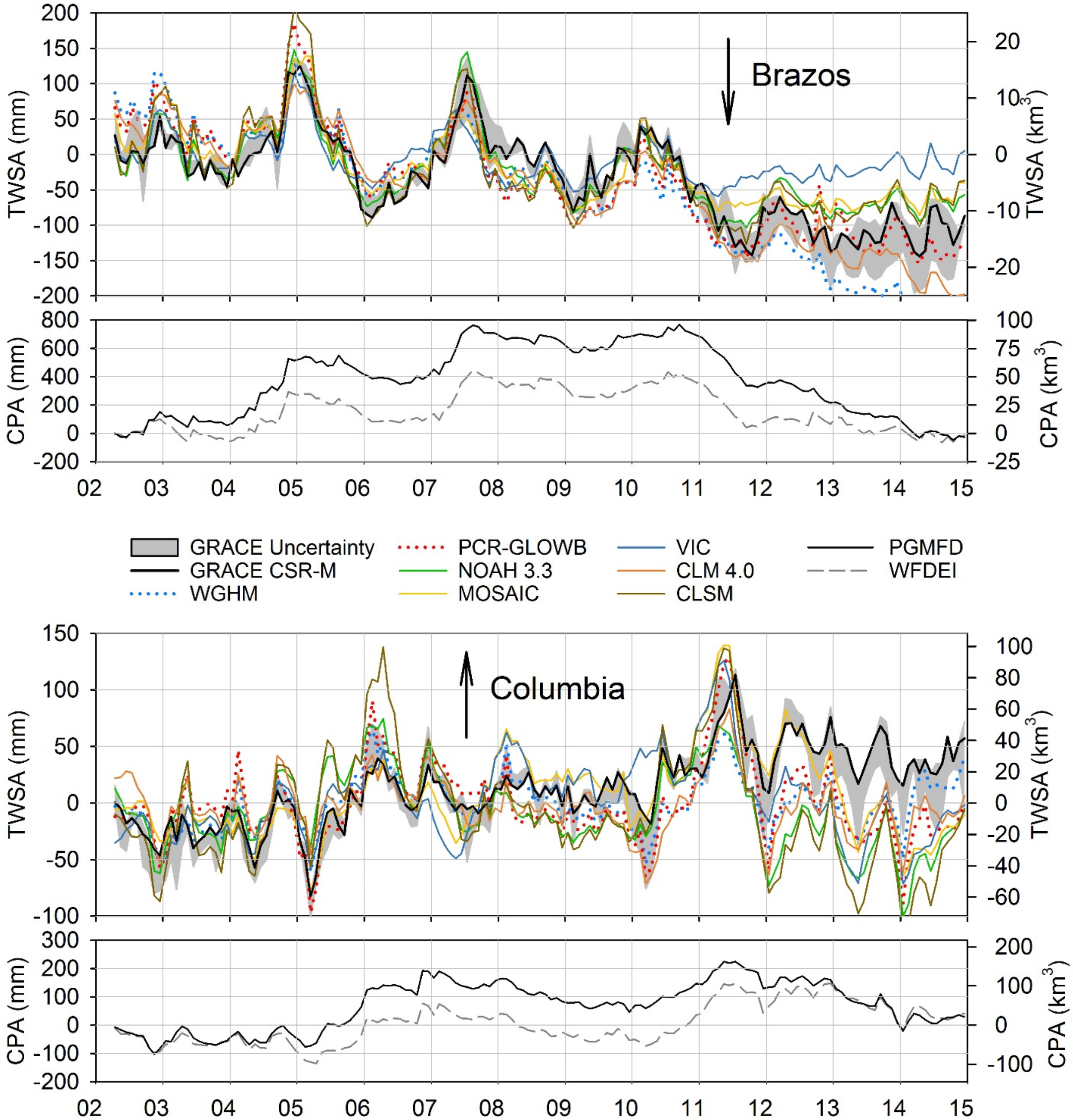

Figure S9 (cted.). Time series of Total Water Storage Anomalies (TWSA) (deseasonalized) for Brazos and Columbia basins and cumulative precipitation anomaly from Princeton Global Meteorological Forcing Dataset (PGMFD) from NOAH-3.3 (GLDAS-2.1) and WFDEI.

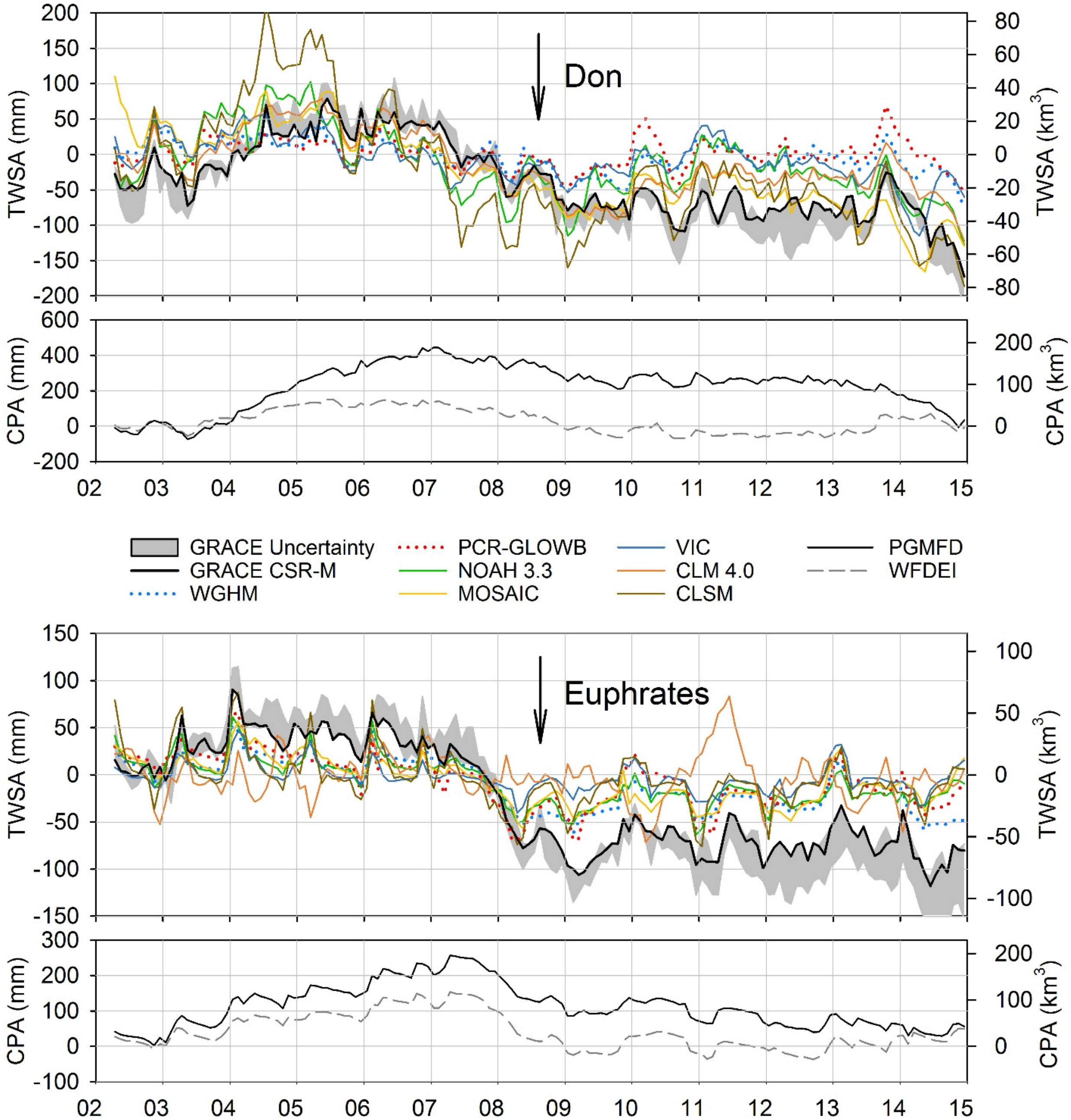

Figure S9 (cted.). Time series of Total Water Storage Anomalies (TWSA) (deseasonalized) for Don and Euphrates basins and cumulative precipitation anomaly from Princeton Global Meteorological Forcing Dataset (PGMFD) from NOAH-3.3 (GLDAS-2.1) and WFDEI.

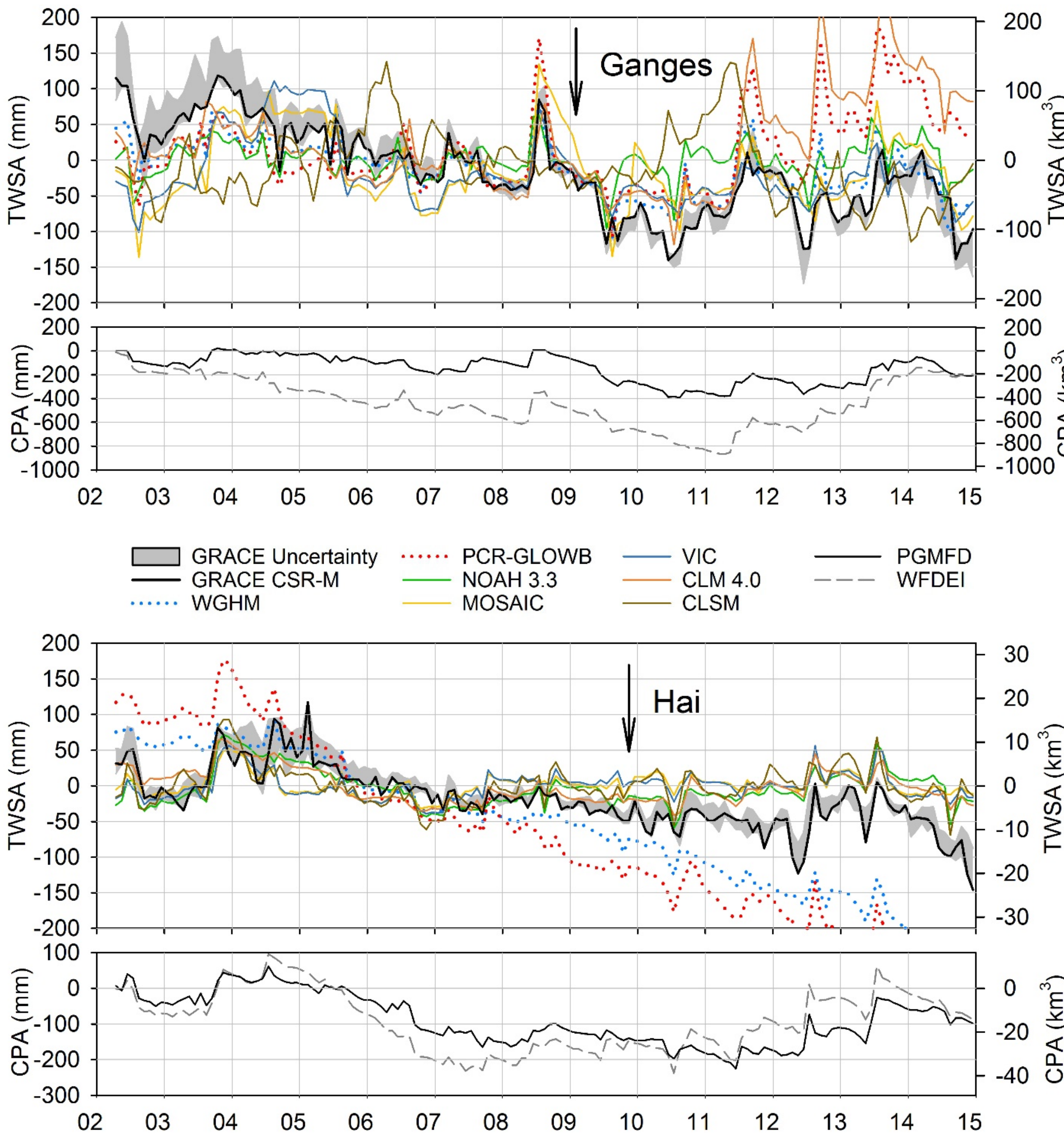

Figure S9 (cted.). Time series of Total Water Storage Anomalies (TWSA) (deseasonalized) for Ganges and Hai basins and cumulative precipitation anomaly from Princeton Global Meteorological Forcing Dataset (PGMFD) from NOAH-3.3 (GLDAS-2.1) and WFDEI.

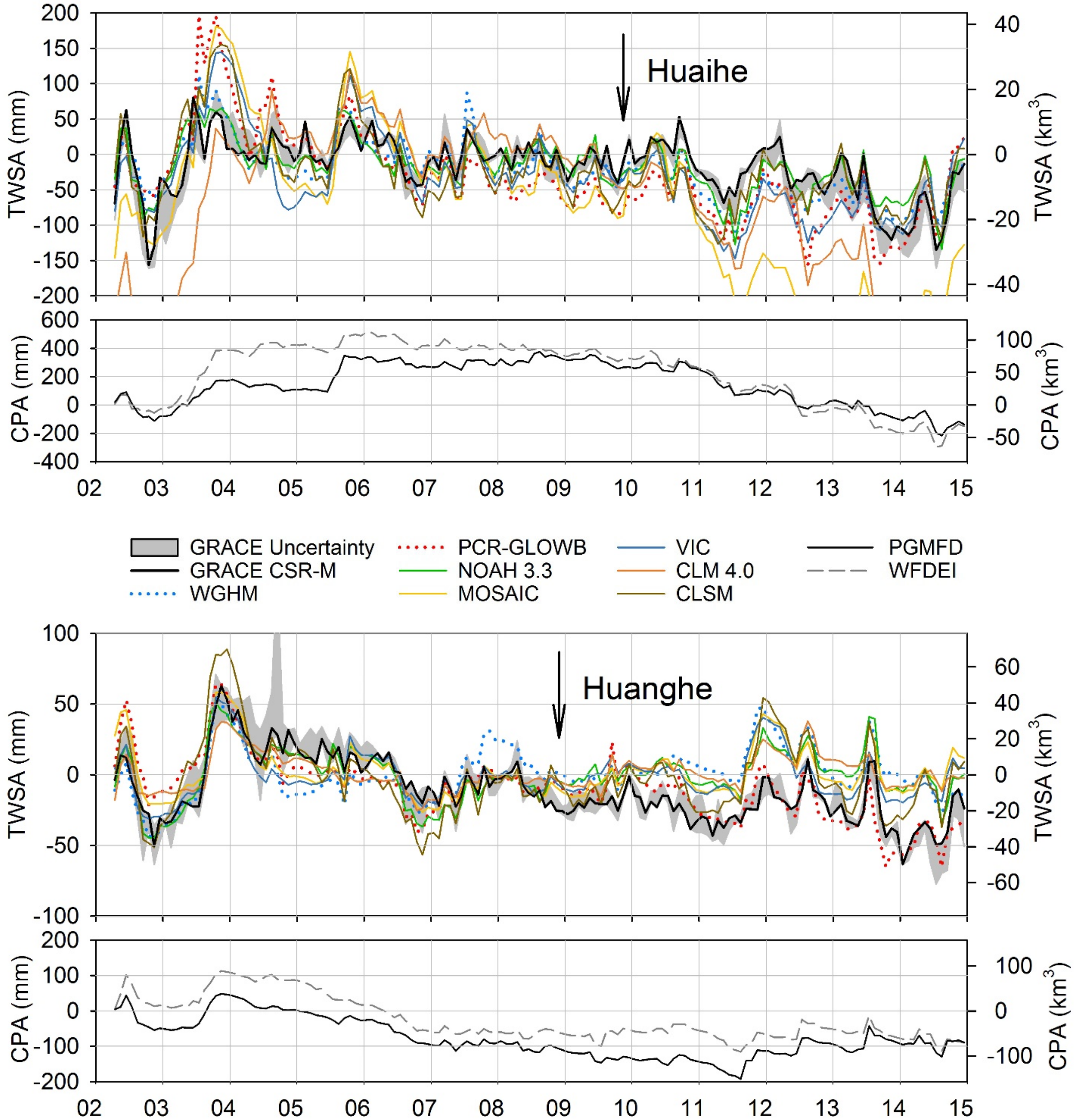

Figure S9 (cted.). Time series of Total Water Storage Anomalies (TWSA) (deseasonalized) for Huanghe and Huaihe basins and cumulative precipitation anomaly from Princeton Global Meteorological Forcing Dataset (PGMFD) from NOAH-3.3 (GLDAS-2.1) and WFDEI.

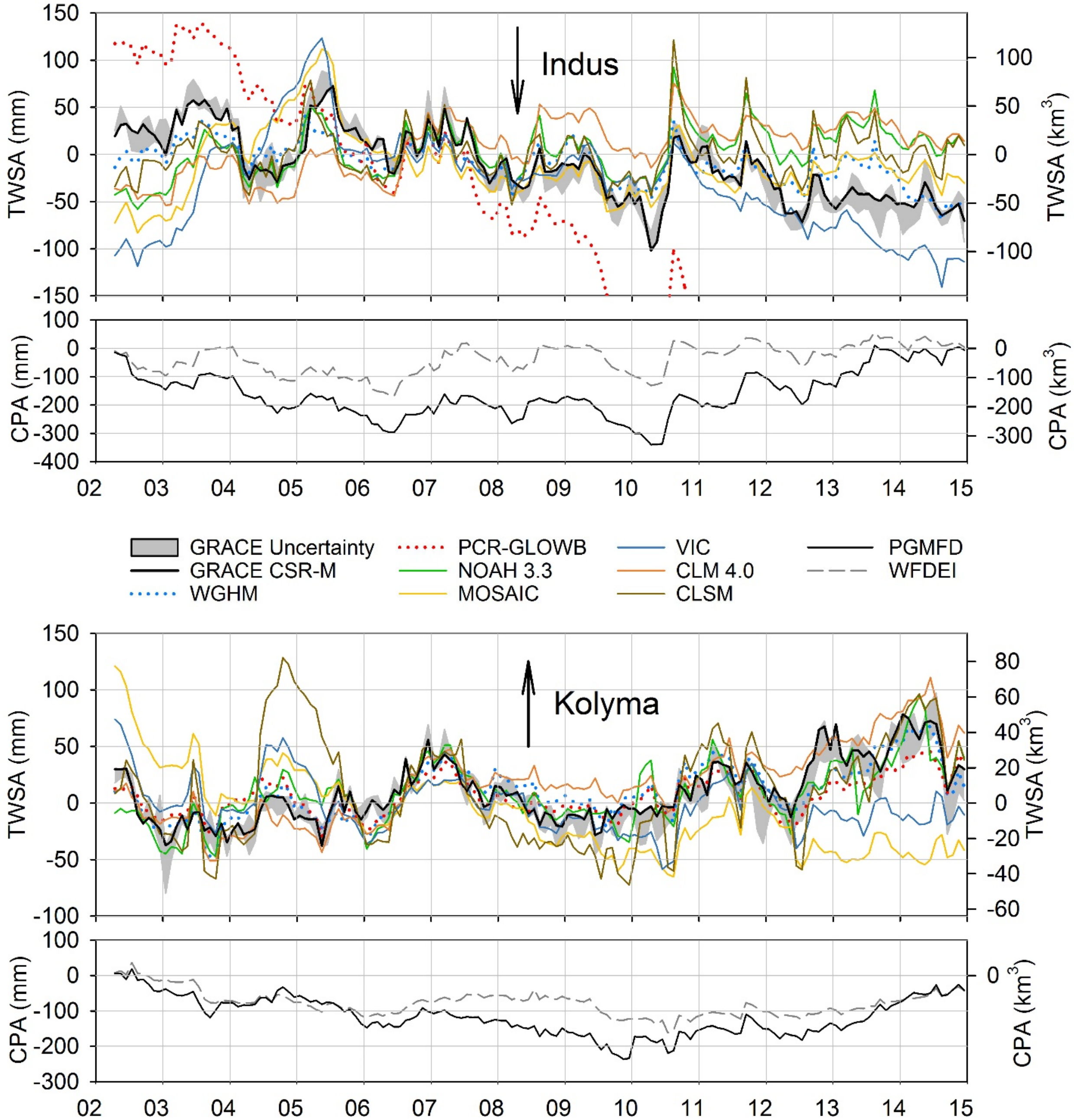

Figure S9 (cted.). Time series of Total Water Storage Anomalies (TWSA) (deseasonalized) for Indus and Kolyma basins and cumulative precipitation anomaly from Princeton Global Meteorological Forcing Dataset (PGMFD) from NOAH-3.3 (GLDAS-2.1) and WFDEI.

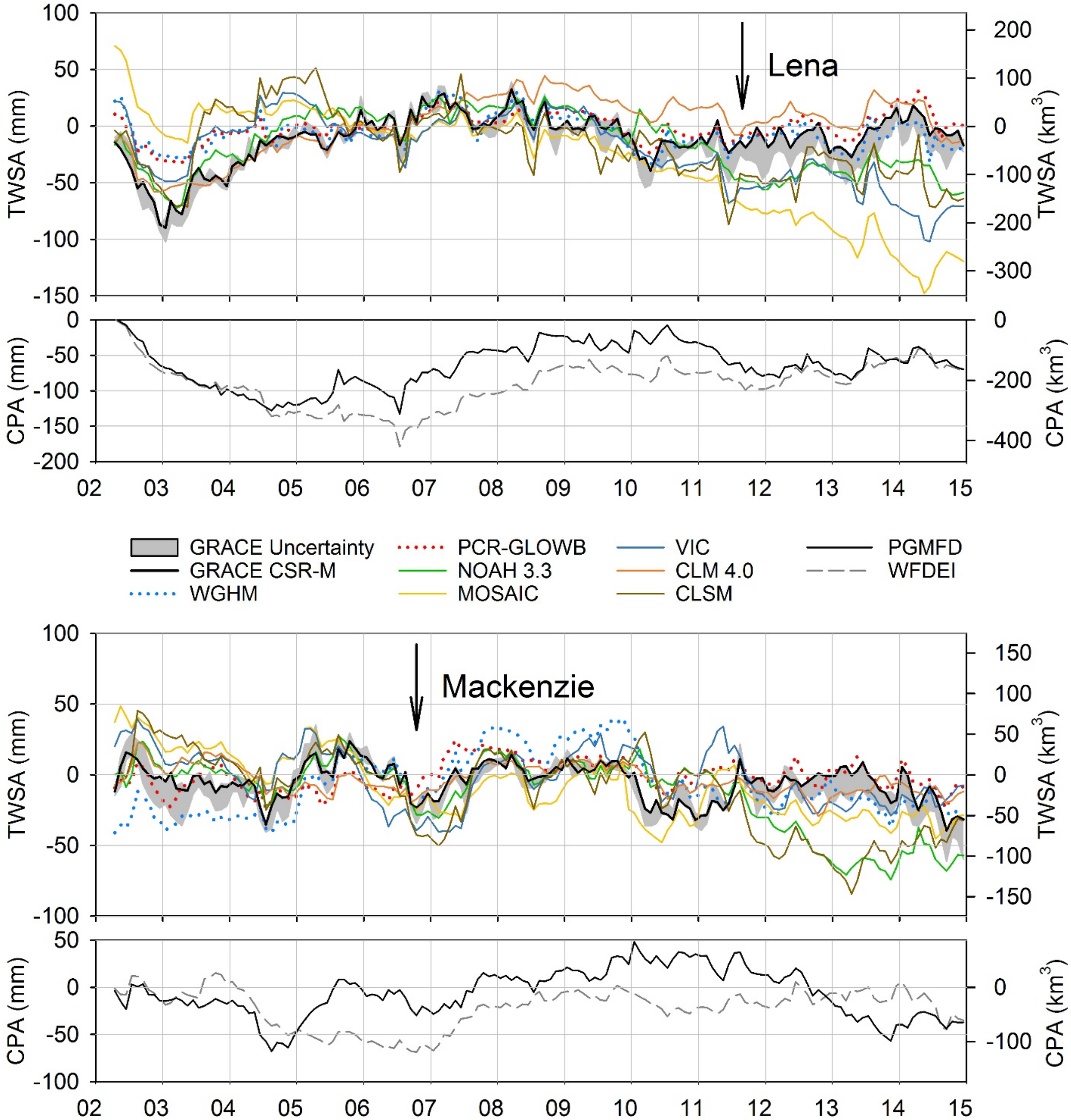

Figure S9 (cted.). Time series of Total Water Storage Anomalies (TWSA) (deseasonalized) for the Lena and Mackenzie basins and cumulative precipitation anomaly from Princeton Global Meteorological Forcing Dataset (PGMFD) from NOAH-3.3 (GLDAS-2.1) and WFDEI.

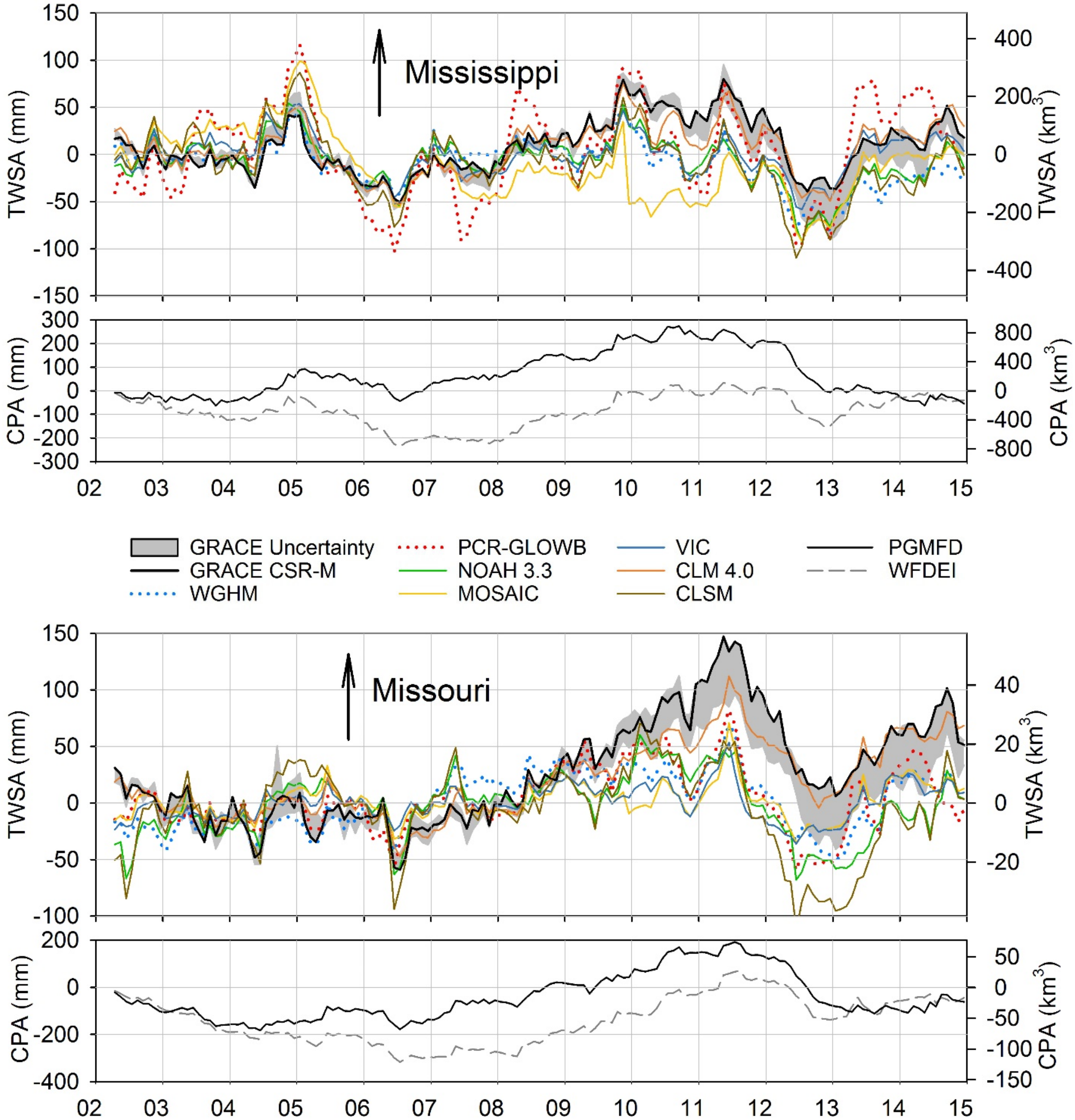

Figure S9 (cted.). Time series of Total Water Storage Anomalies (TWSA) (deseasonalized) for the Mississippi and Missouri basins and cumulative precipitation anomaly from Princeton Global Meteorological Forcing Dataset (PGMFD) from NOAH-3.3 (GLDAS-2.1) and WFDEI.

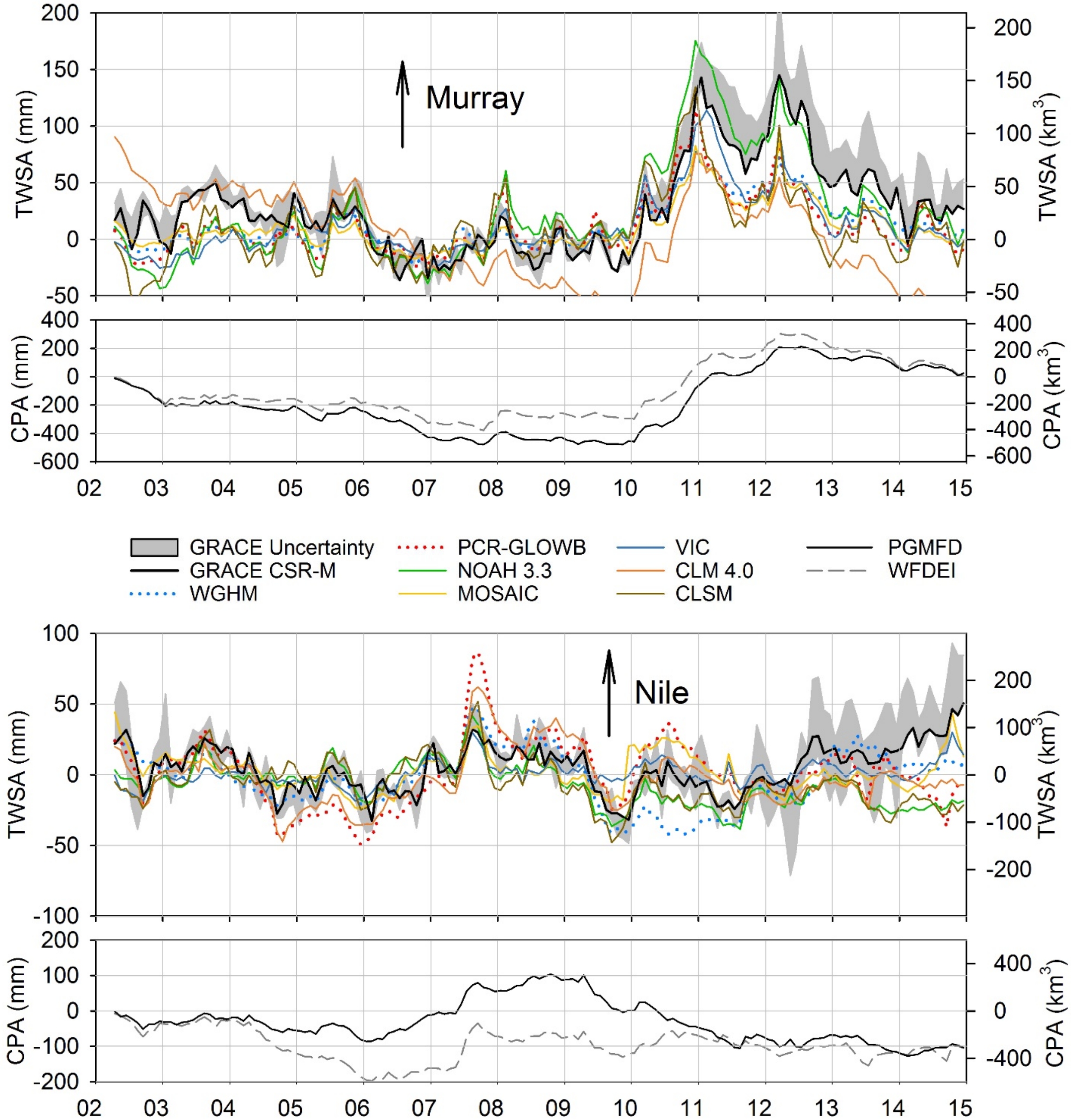

Figure S9 (cted.). Time series of Total Water Storage Anomalies (TWSA) (deseasonalized) for Nile and Murray basins and cumulative precipitation anomaly from Princeton Global Meteorological Forcing Dataset (PGMFD) from NOAH-3.3 (GLDAS-2.1) and WFDEI.

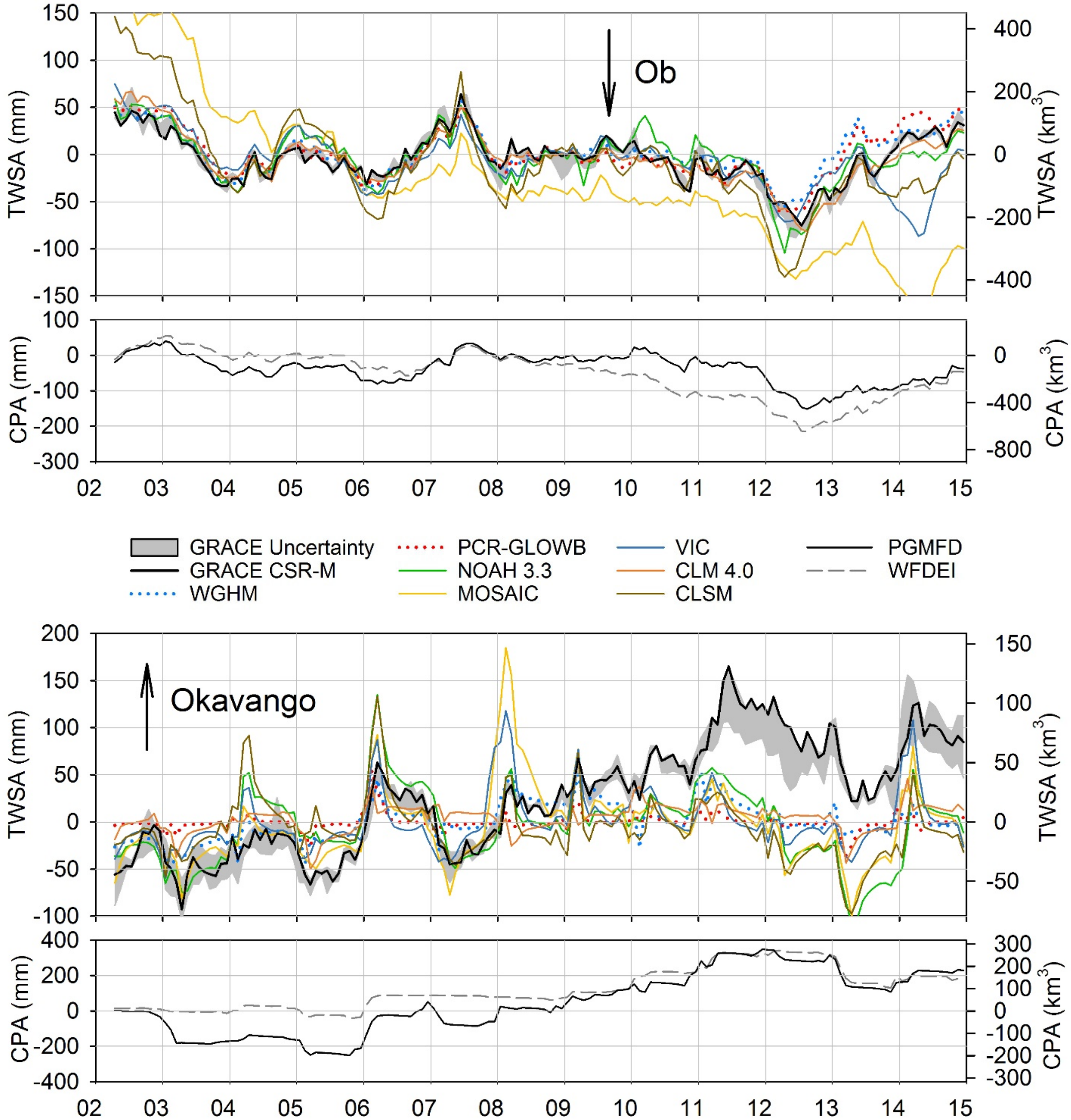

Figure S9 (cted.). Time series of Total Water Storage Anomalies (TWSA) (deseasonalized) for the Ob and Okavango basins and cumulative precipitation anomaly from Princeton Global Meteorological Forcing Dataset (PGMFD) from NOAH-3.3 (GLDAS-2.1) and WFDEI.

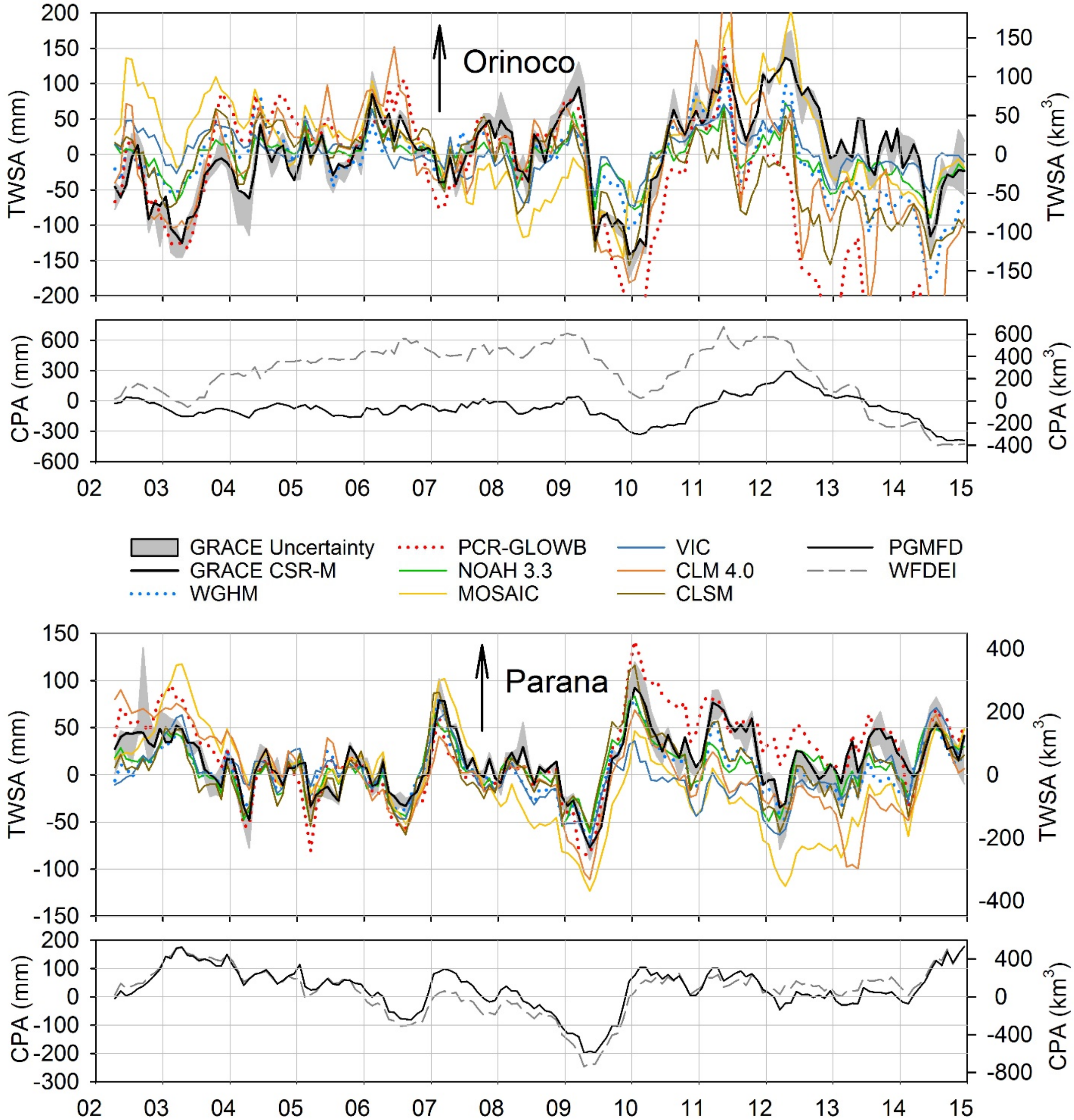

Figure S9 (cted.). Time series of Total Water Storage Anomalies (TWSA) (deseasonalized) for the Orinoco and Parana basins and cumulative precipitation anomaly from Princeton Global Meteorological Forcing Dataset (PGMFD) from NOAH-3.3 (GLDAS-2.1) and WFDEI.

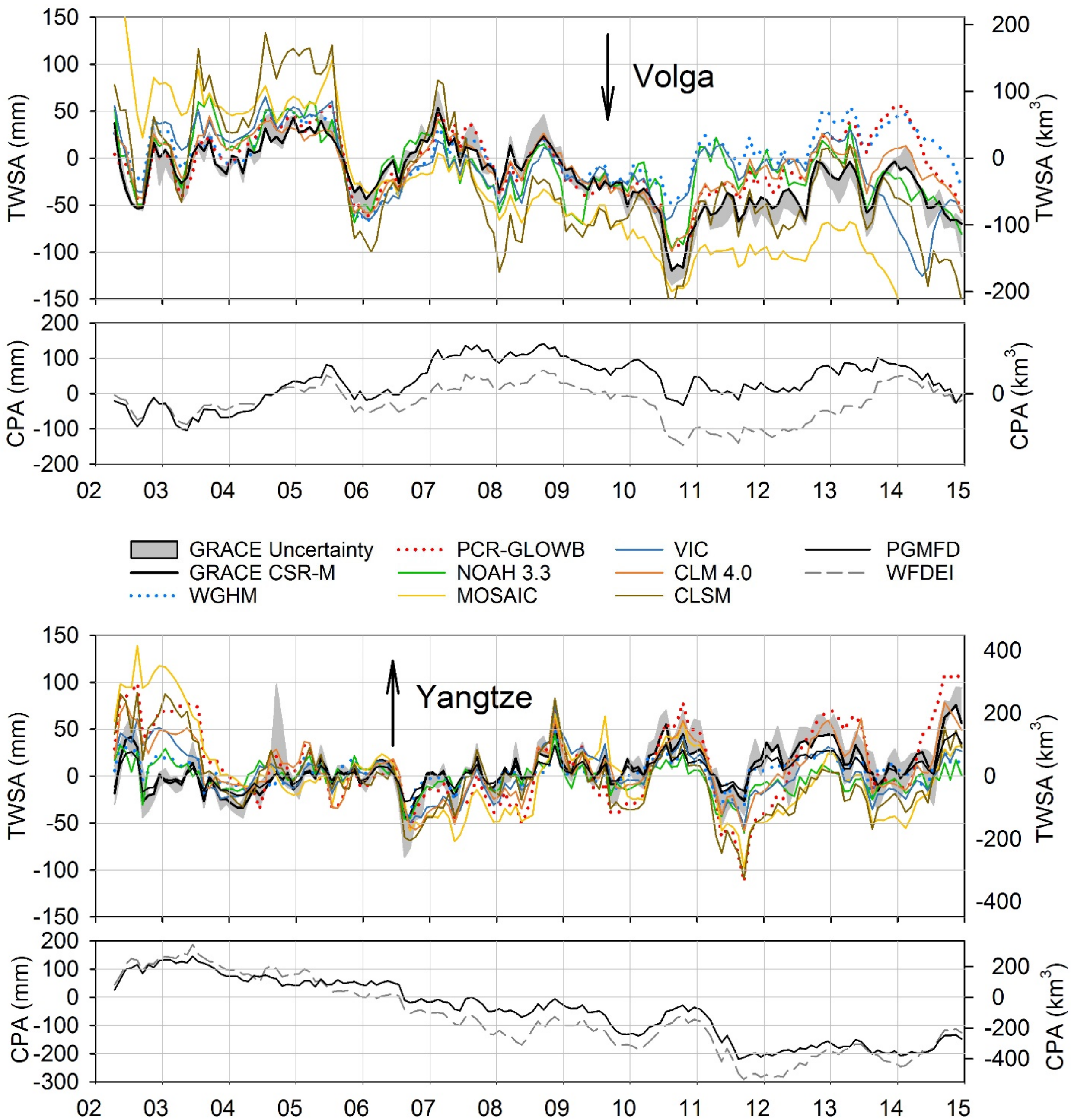

Figure S9 (cted.). Time series of Total Water Storage Anomalies (TWSA) (deseasonalized) for the Volga and Yangtze basins and cumulative precipitation anomaly from Princeton Global Meteorological Forcing Dataset (PGMFD) from NOAH-3.3 (GLDAS-2.1) and WFDEI.

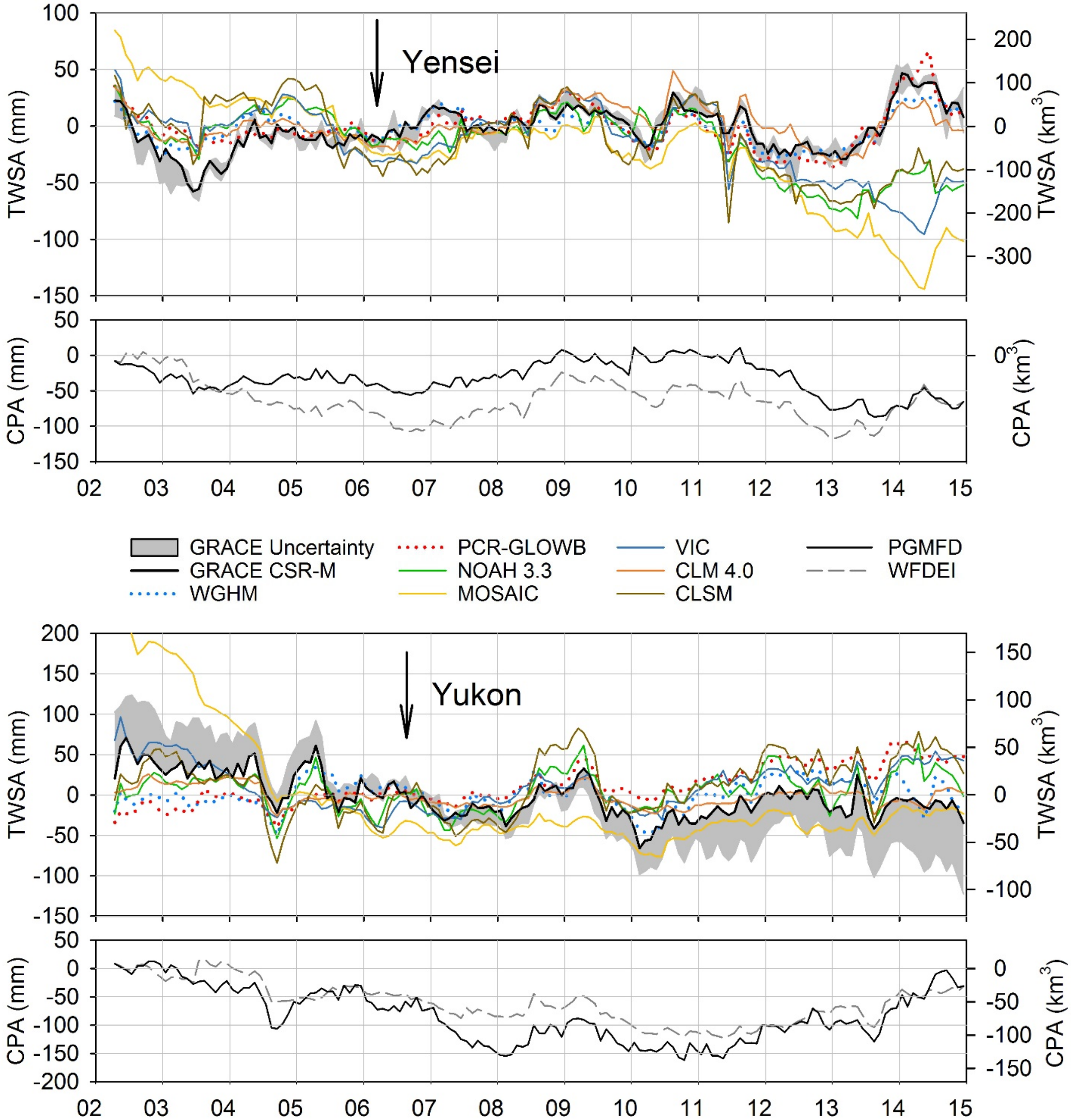

Figure S9 (cted.). Time series of Total Water Storage Anomalies (TWSA) (deseasonalized) for the Yenisei and Yukon basins and cumulative precipitation anomaly from Princeton Global Meteorological Forcing Dataset (PGMFD) from NOAH-3.3 (GLDAS-2.1) and WFDEI.

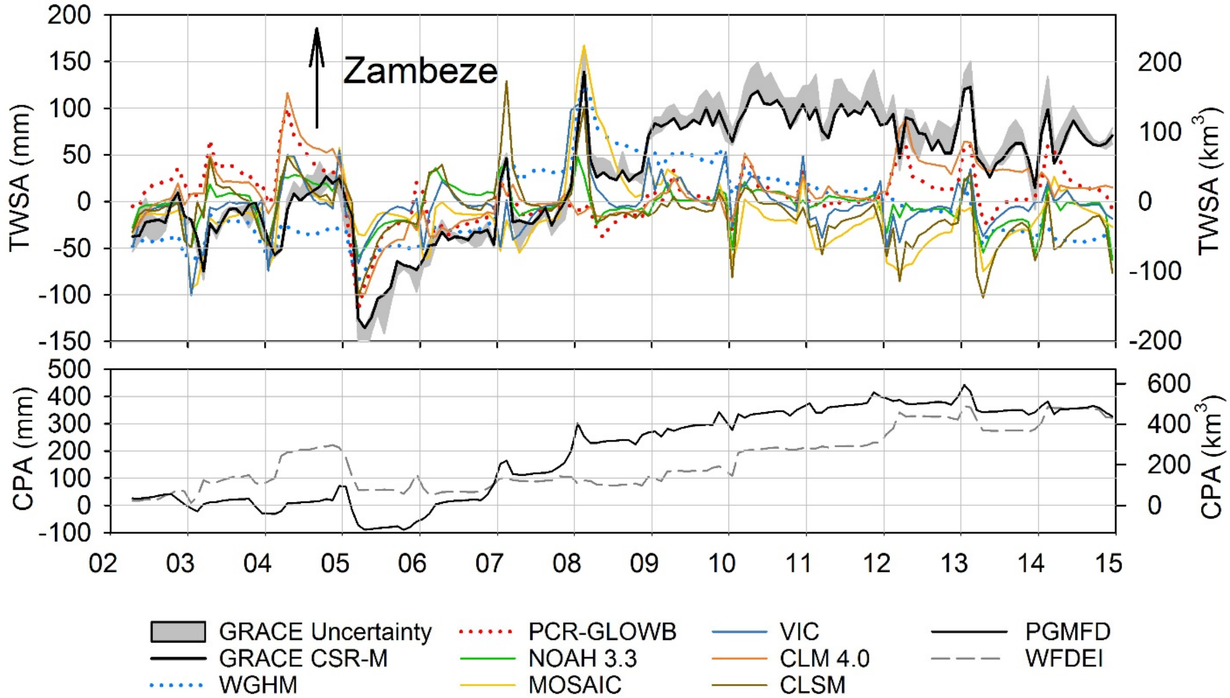

Figure S9 (cted.). Time series of Total Water Storage Anomalies (TWSA) (deseasonalized) for the Zambezi basin and cumulative precipitation anomaly from Princeton Global Meteorological Forcing Dataset (PGMFD) from NOAH-3.3 (GLDAS-2.1) and WFDEI.

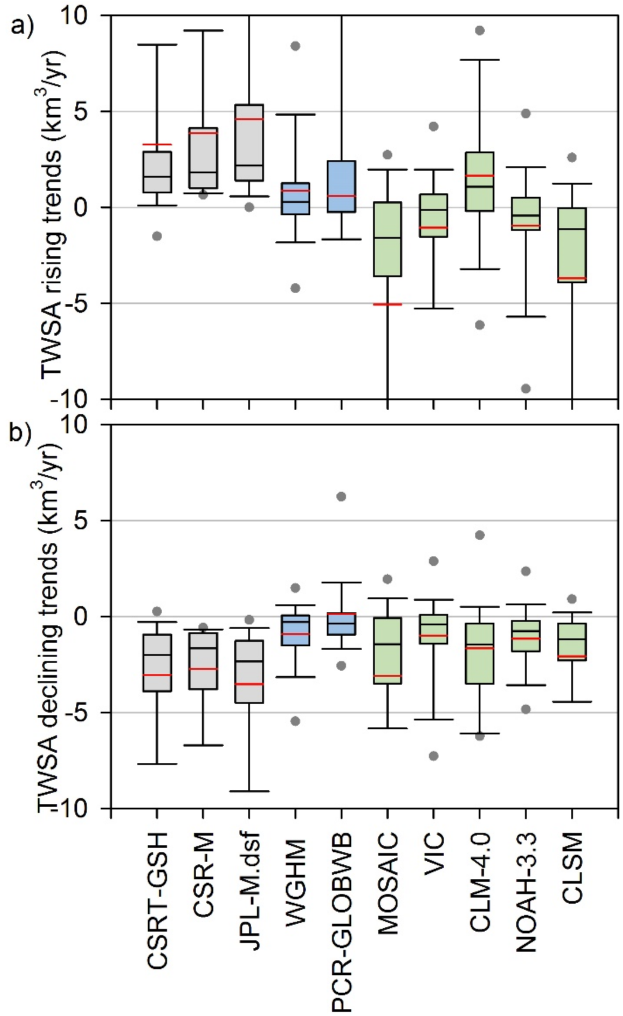

Figure S10. Boxplot showing basic statistics of GRACE and modeled TWSA trends for rising trends (GRACE CSR-M ≥0.5 km^3/yr) and declining trends (CSR-M ≤-0.5 km^3/yr). Boxplots include median (black horizontal line, mean red line, interquartile range (25 – 75 percentiles, box), 10^{th} – 90^{th} percentiles (bars) and 5^{th} – 95^{th} percentiles (points). The GRACE solutions include CSRT-GSH.sf; CSR-M, and JPL-M.dsf (downscaled), GHWRMs (WGHM and PCR-GLOBWB), and LSMs (GLDAS-1.0 MOSAIC and VIC; GLDAS-2.1, NOAH-3.3 and CLSM) and CLM-4.0.

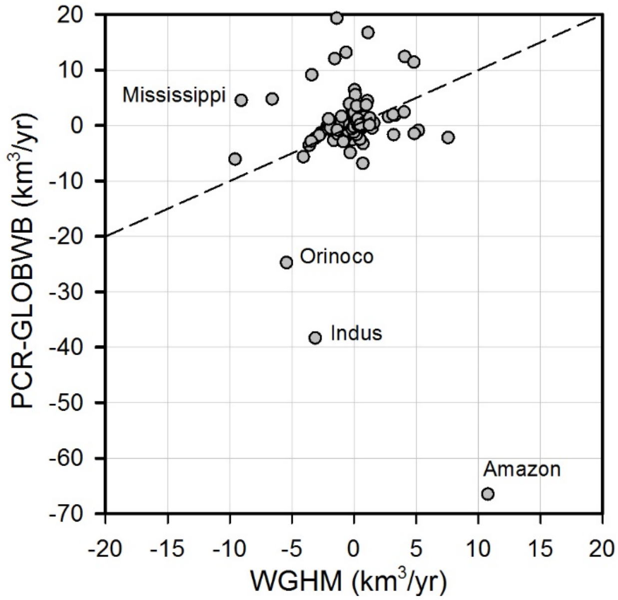

Figure S11. Comparison of TWSA trends from PCR-GLOBWB relative to those from WGHM showing large differences in certain basins, such as the Amazon, Indus, and Orinoco basins. For trends, see Fig. 5.

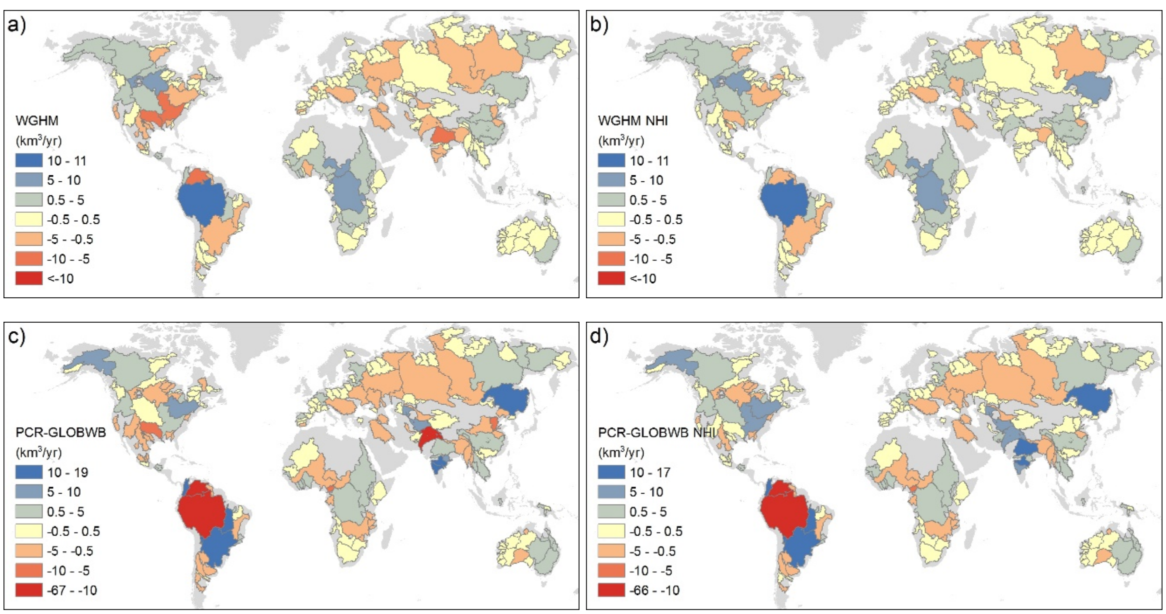

Figure S12. Comparison between a) WGHM with human intervention (WGHM) and (b) WHGM with no human intervention (NHI). Similar plots for (c) PCR-GLOBWB and (d) PCR-GLOBWB-NHI.

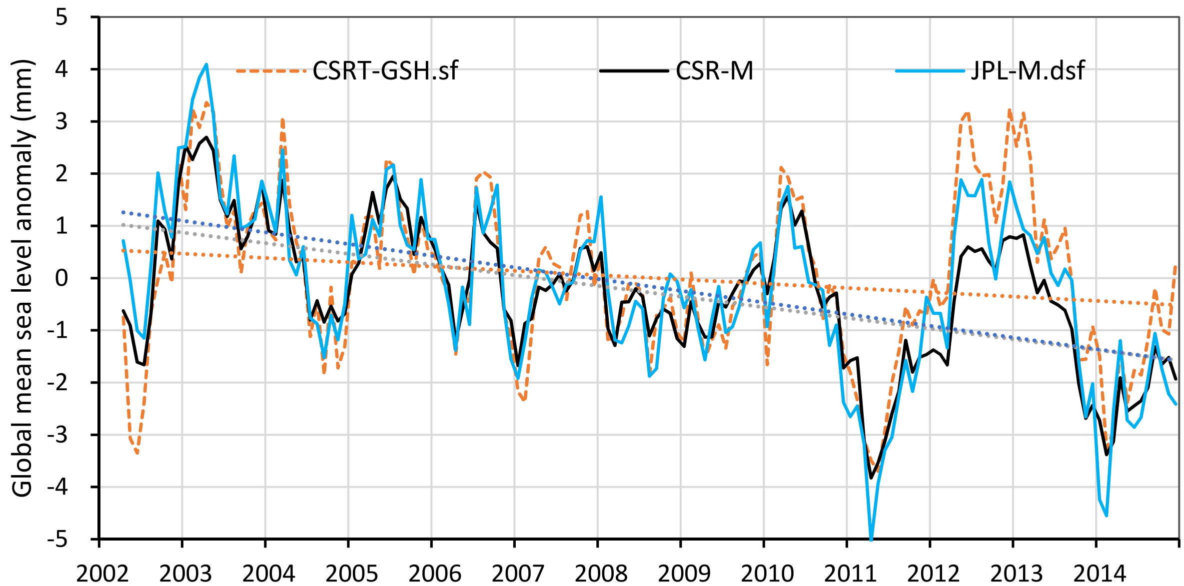

Figure S13. Global mean sea level anomaly derived from GRACE TWSA, including CSR and JPL (downscaled, dsf) mascons solutions (CSR-M and JPL-M) and CSR Tellus gridded spherical harmonic solution rescaled (CSRT-GSH.sf). TWSA derived from GRACE (km^3/yr) was divided by the area of the oceans (361×10^6 km^3) to estimate the contribution of TWSA to GMSL.

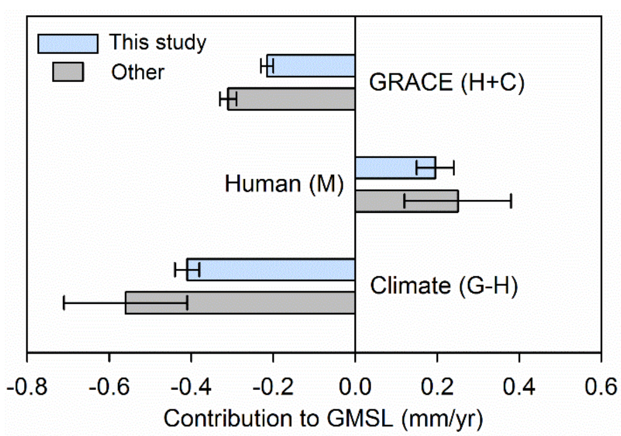

Figure S14. Contributions of land water storage trends to global mean sea level (GMSL) from this study and from the literature with similar time periods (2002–2014). The corresponding data and sources are provided in Table S12. GRACE TWSA trends include human and climate impacts and show similar results for this study relative to previous studies. Human impacts are derived from models (WGHM and PCR-GLOBWB runs with and without human intervention in this study). Human impacts from the literature include IPCC (68) and Wada et al. (69). Climate contributions to land water storage and GMSL were estimated by subtracting contributions from human intervention from GRACE trends. Results show that GRACE and climate contribute negatively to GMSL (reducing the rate of global sea level rise) whereas human impacts contribute positively to GMSL (increasing rate of global sea level rise). The impacts of climate are about a factor of 2 greater than those of human intervention.

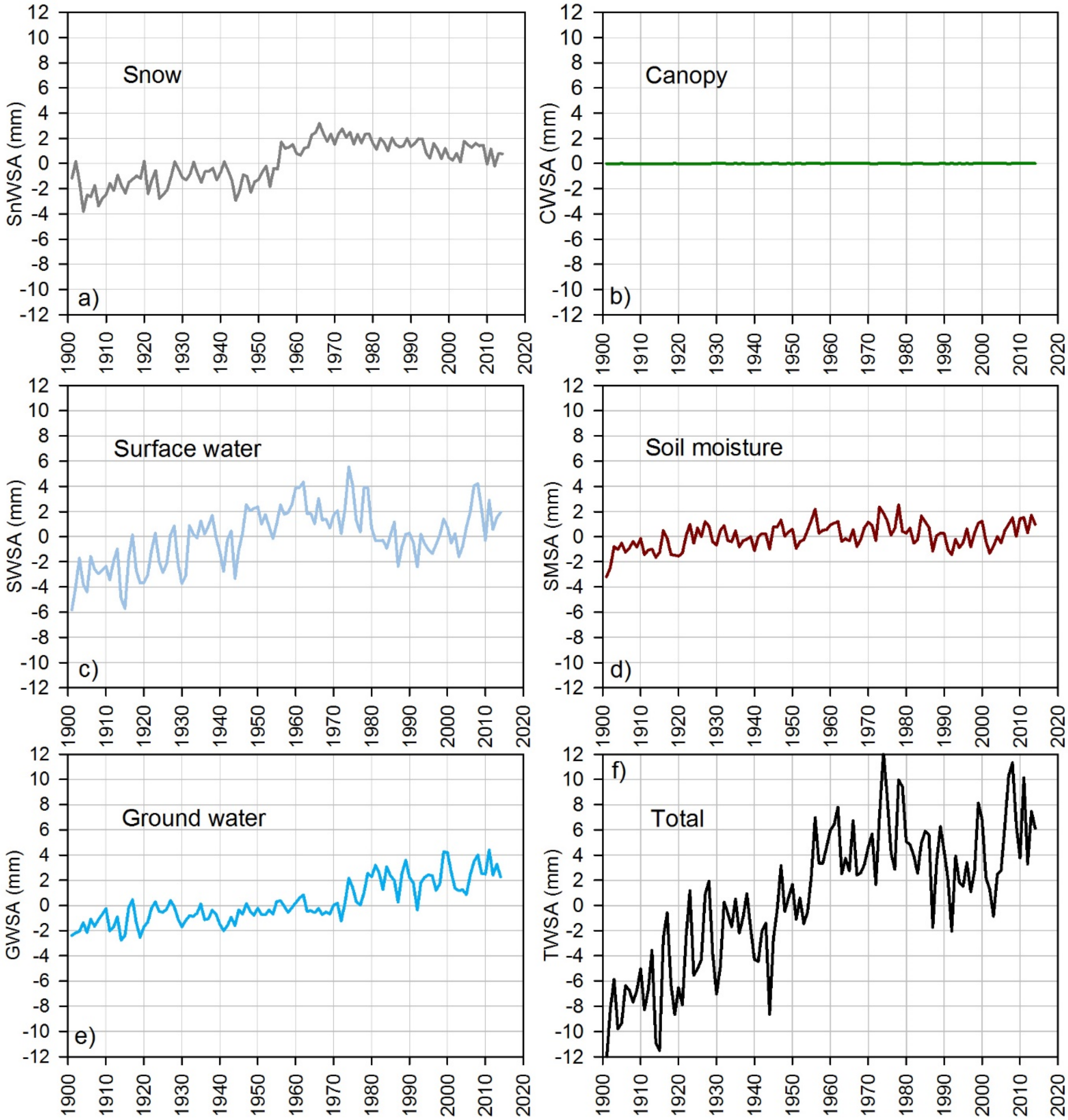

Figure S15. Timeseries of component and total water storage anomalies to evaluate spin-up in the WGHM model. SnWSA: snow water storage anomaly; CWSA, canopy water storage anomaly; SWSA, surface water storage anomaly; SMSA, soil moisture storage anomaly; GWSA, Ground water storage anomaly; TWSA, total water storage anomaly.

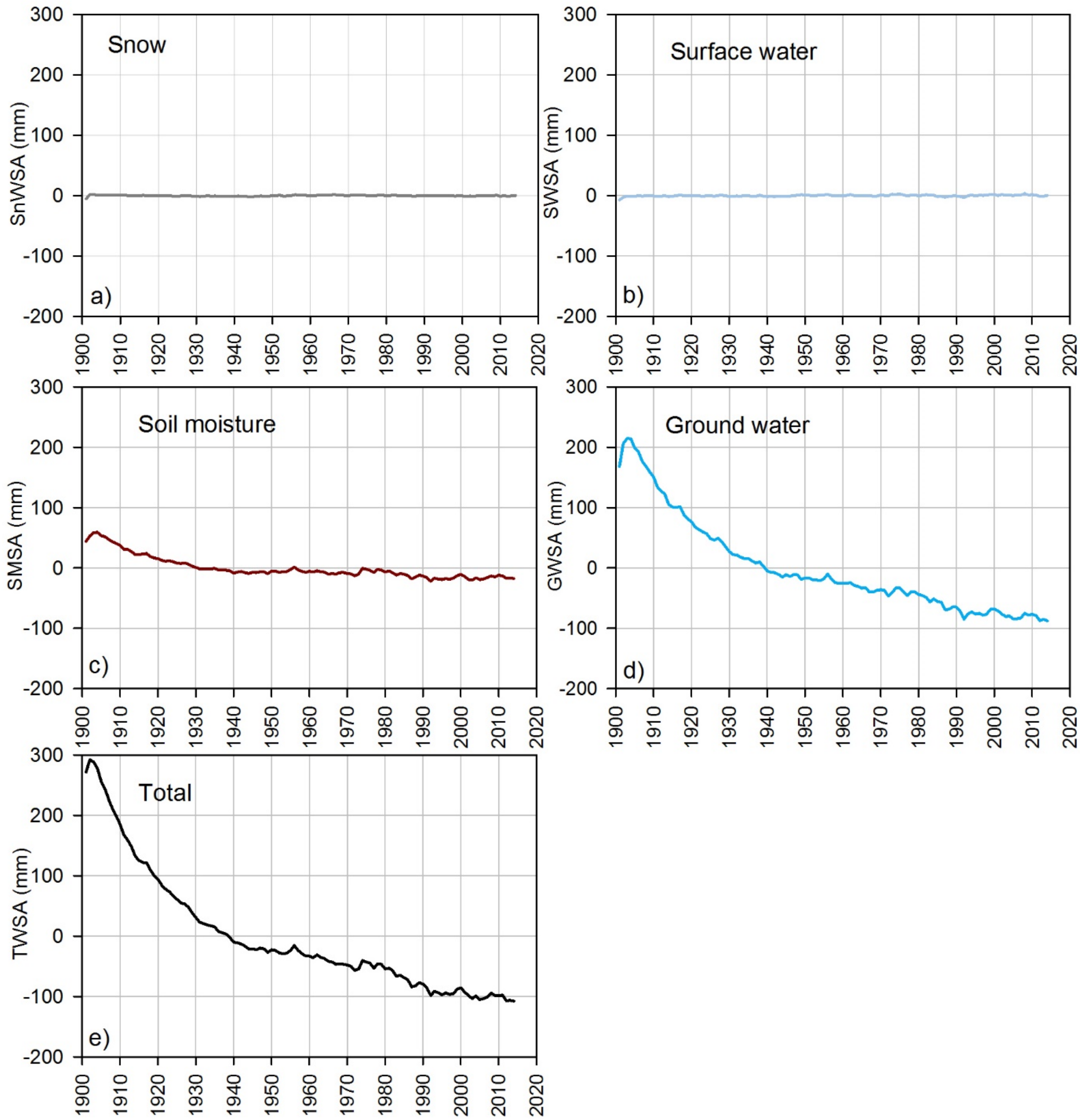

Figure S16. Timeseries of component and total water storage anomalies to evaluate spin-up in the CLM-4.0 model. SnWSA: snow water storage anomaly; SWSA, surface water storage anomaly; SMSA, soil moisture storage anomaly; GWSA, Ground water storage anomaly; TWSA, total water storage anomaly.

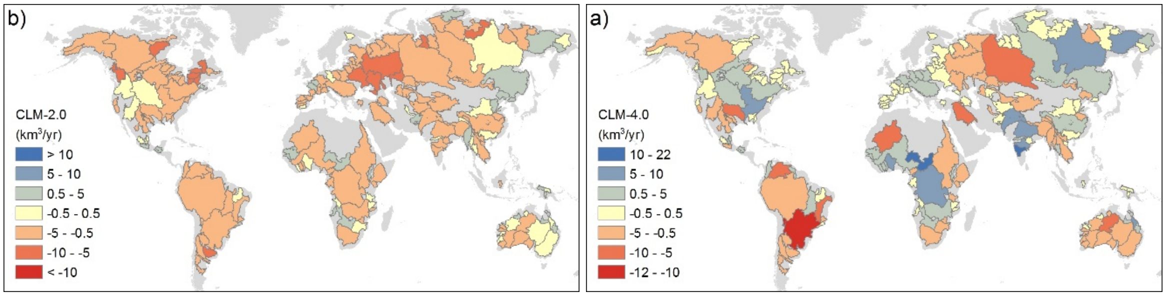

Figure S17. Comparison of TWSA trends from an early version of the CLM model (CLM-2.0; GLDAS 1.0 suite) and a recent version of the model (CLM-4.0).

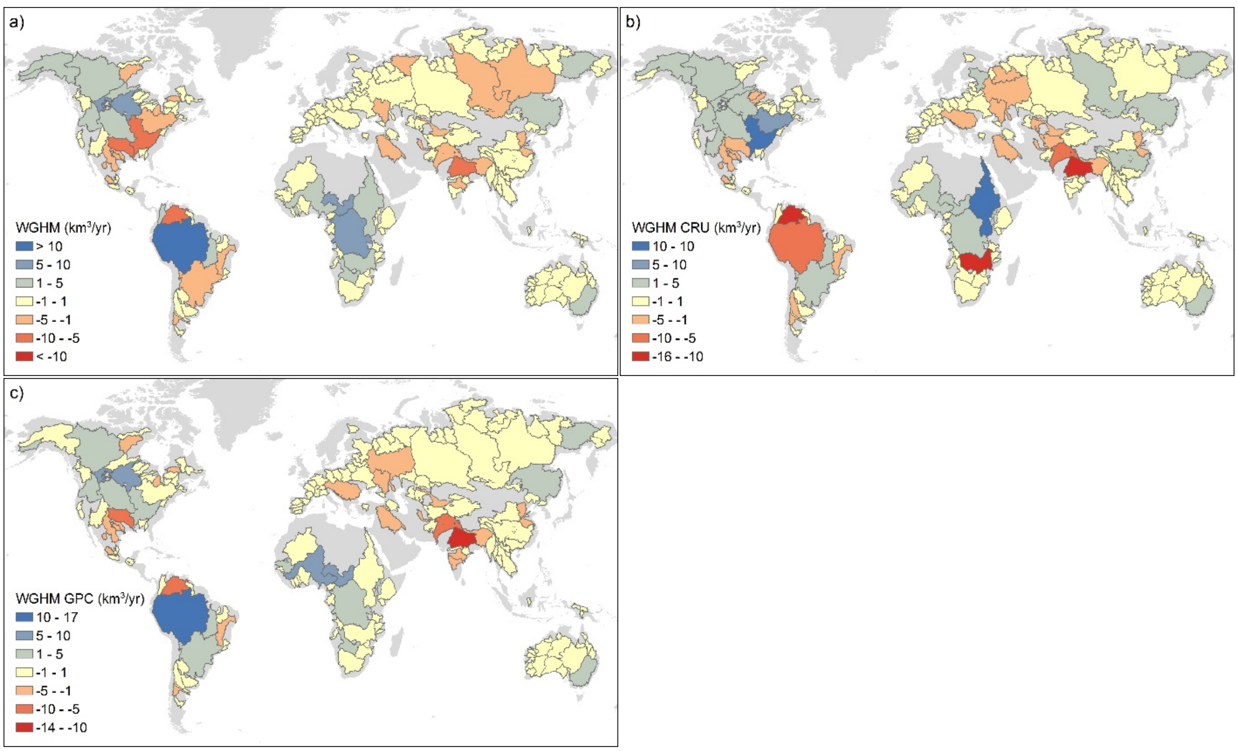

Figure S18. Comparison in TWSA trends from a) WGHM with WFDEI climate forcing, b) WGHM with CRU forcing, and c) WGHM with GPCC forcing. All forcings used for WGHM are available at 0.5˚ x 0.5˚ resolution. Monthly CRU TS 3.23 (70) values of precipitation, number of rain days, temperature and cloudiness were used together with a temporal disaggregation scheme (12) to obtain daily values (variant CRU). CRU is available from 1901-2014. For forcing variant GPCC, we used GPCC v.7 (71) monthly totals instead of CRU for the years that are available 1901-2013, for 2014 we used CRU TS 3.23 instead. WATCH Forcing Data based on ERA-Interim reanalysis (WFDEI, (20) daily forcing variables precipitation (bias corrected to monthly GPCC for 1901-2013 and CRU for 2014), temperature, shortwave downwelling and longwave downwelling radiation was used. Differences are high in particular for the station density of precipitation, not very much for total sums (73; Table 4) in the input data, but largely due to the applied undercatch correction method (72, 73).

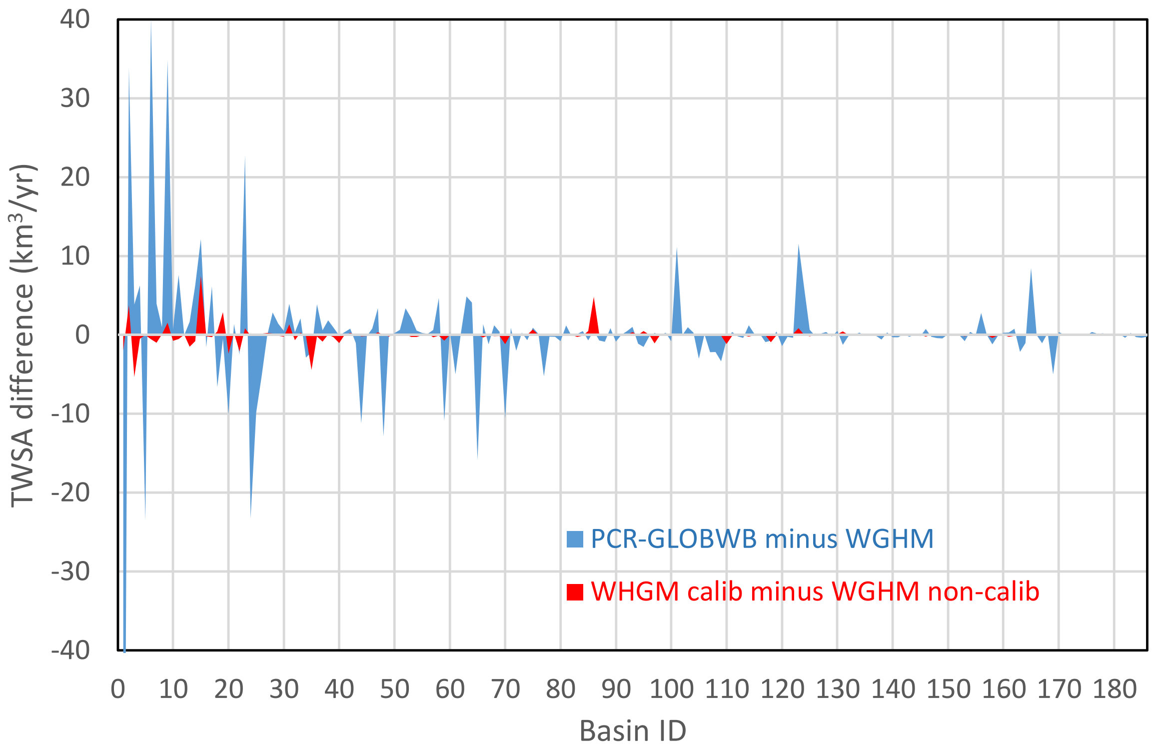

Figure S19. Comparison of the differences between GHWRMs (PCR-GLOBWB minus WGHM, blue) relative to the difference between calibrated and non-calibrated WGHM runs (red). The result shows that the differences between the two models are much greater than the difference between the calibrated and non-calibrated WGHM; therefore, calibration alone cannot account for the differences between the GHWRMs.

Table S2. (a) Description of models used in this study.

MODEL >	*WGHM*	*PCR-GLOBWB*	*NOAH GLDAS 1.0*	*NOAH-3.3* GLDAS 2.1	*MOSAIC* GLDAS 1	*VIC* GLDAS 1	*CLM* GLDAS 1	*CLSM* GLDAS 2.1	*CLM*
Version	2.2		2.7	3.3			2.0	Fortuna 2.5	4.0
Spatial resolution (deg)	0.5	0.5	1	1	1	1	1	1	1
Spatial res. (km equator)	55	55	110	110	110	110	110	110	110
Time resolution simulation time step	monthly daily	monthly daily	monthly 3 hr	monthly 3 hr	monthly 3 hr	monthly 3 hr	monthly 3 hr	monthly 1 hr	monthly 3 hr
Time span	1950-2014	1958-2014	1979-present	2000-present	1979-present	1979-present	1979-present	2001-present	1979 - 2014
Subgrid variability	yes	yes	1-13 tiles	1-13 tiles	1-13 tiles	1-13 tiles	1-13 tiles	1-13 tiles	1-13 tiles
Surface water storage	yes	yes	no	no	no	no	no	no	yes
Canopy Storage	yes	yes	yes	yes	yes	yes	yes	yes	yes
Vegetation	yes	yes	SVAT	SVAT	SVAT	SVAT	SVAT	SVAT	SVAT
Irrigation	yes	yes	no	no	no	no	no	no	no
Soil water storage	yes	yes	yes	yes	yes	yes	yes	yes	yes
Soil layers (no.)	1	2	4	4	3	3	10	10	10
Soil data			(1)	(1)	(1)	(1)	(1)	(1)	(1)
Soil zone depth (m)	2	2	3.5	3.5	1.9	3.5	3.4	3.4	3.4
Groundwater storage	yes	yes	no	no	no	no	no	yes	yes
Precipitation data	WFDEI	WFDEI	(2)	(2)	(3)	(3)	(3)	(3)	(4)
ET	Priestley Taylor	FAO 56 PM	Energy balance	Energy balance	Energy balance	Energy balance	Energy balance	Energy balance	Energy balance
Runoff	SE, IE	SE, IE	SE, IE	SE, IE	SE, IE	SE, IE	SE, IE	SE, IE	SE, IE
Surface flow routing	yes	yes	no	no	no	no	no	no	yes
Water balance	yes	yes	yes	yes	yes	yes	yes	yes	yes
Calibration/Data Assimilation	yes	no	no	no	no	no	no	no	no
Human water use	yes	yes	no	no	no	no	no	no	no

SVAT: soil vegetation atmosphere transfer scheme; WFDEI: Watch Forcing Data + Era Interim Reanalysis; PM: Penman Monteith; Energy balance in model framework; Runoff: SE: saturation excess; IE, infiltration excess; PET, potential ET; RS: remote sensing; data assimilation in GLDAS models may be considered a type of calibration.

Precipitation forcing: (2) NOAA Climate Prediction Center Merged Analysis of Precipitation; (3) Princeton Global Meteorological Forcing Dataset, (4) CRU-NCEP.

Soil data source (34).

Table S2 (b) Description of number of soil layers, total depths, and depths of soil layers in GLDAS – 1.0 land surface models. NOAH-3.3 in GLDAS-2.1 has the same soil depth and intervals as NOAH-2.7. CLM-4.0 has the same soil depth and intervals as CLM-2.0.

Data set	*Model*	*No. soil layers and (total depth, m)*	*Soil layer*	
			cm	*cm*
GLDAS-1	NOAH-2.7 NOAH-3.3	4 (2.0)	0-10	10-40
			40-100	100-200
	Mosaic	3 (3.5)	0-2	2-150
			150-350	
	VIC	3 (1.9)	0-10	10-160
			160-190	
	CLM-2.0 CLM-4.0	10 (3.4)	0-1.8	1.8-4.5
			4.5-9.1	9.1-16.6
			16.6-28.9	28.9-49.3
			49.3-82.9	82.9-138.3
			138.3-229.6	229.6-343.3
GLDAS-2.1	CLSM-F2.5	1 (1.0)	0-100	

Table S3. River Basin ID, name, basin area based on TRIP database, aridity index (AI) and climate setting (H, humid; SH, subhumid; SA, semiarid; A, arid) and percent of basin area that is irrigated.

ID	*River Name*	*Area (10^6 km^2)*	*AI*	*Clim.*	*Irrig (%)*
1	Amazon	6.234	1.25	H	0.15
2	Congo	3.759	0.89	H	0.01
3	Mississippi	3.253	0.68	H	3.92
4	Ob	2.997	0.76	H	0.23
5	Paraná	2.988	0.76	H	0.87
6	Nile	2.978	0.34	SA	1.77
7	Yenisei	2.609	0.88	H	0.03
8	Lena	2.346	0.77	H	0.00
9	Niger	2.124	0.34	SA	0.18
10	Amur	1.868	0.83	H	2.04
11	Yangtze	1.831	1.01	H	8.40
12	Tamanrasset	1.762	0.02	A	0.01
13	MacKenzie	1.740	0.76	H	0.00
14	Volga	1.407	0.89	H	0.50
15	Zambezi	1.341	0.55	SH	0.30
16	Lake Eyre	1.248	0.13	A	0.00
17	Nelson	1.110	0.67	H	0.60
18	St. Lawrence	1.109	1.10	H	0.48
19	Murray	1.070	0.36	SA	2.46
20	Ganges	1.032	0.73	H	30.62
21	Orange	0.999	0.22	SA	0.63
22	Indus	0.971	0.39	SA	22.71
23	Chari	0.925	0.40	SA	0.13
24	Orinoco	0.912	1.34	H	0.94
25	Tocantins	0.876	0.99	H	0.21
26	Yukon	0.851	0.69	H	0.00
27	Danube	0.806	0.91	H	4.78
28	Mekong	0.804	0.99	H	3.77
29	Victoria Wiso	0.790	0.19	A	0.00
30	Okavango	0.793	0.29	SA	0.02
31	Huáng Hé	0.786	0.52	SH	9.19
32	Euphrates	0.762	0.27	SA	10.15
33	Jubba	0.741	0.26	SA	0.17
34	Columbia	0.722	0.78	H	3.98
35	Arkansas	0.667	0.61	SH	3.78
36	Brahmaputra	0.657	1.19	H	6.55

ID	*River Name*	*Area (10^6 km^2)*	*AI*	*Clim.*	*Irrig (%)*
37	Kolyma	0.640	0.75	H	0.00
38	Colorado	0.636	0.27	SA	2.27
39	Rio Grande	0.616	0.26	SA	1.91
40	São Francisco	0.614	0.55	SH	1.03
41	Nullarbor	0.553	0.13	A	0.00
42	Dnieper	0.514	0.78	H	2.69
43	Salt Lake	0.494	0.15	A	0.00
44	Amu Darya	0.493	0.54	SH	8.92
45	De Grey	0.472	0.14	A	0.00
46	Limpopo	0.444	0.33	SA	0.80
47	Senegal	0.443	0.28	SA	0.32
48	Tarim	0.440	0.10	A	1.95
49	Don	0.425	0.62	SH	1.50
50	Syr Darya	0.418	0.29	SA	7.90
51	Xi	0.407	1.17	H	7.08
52	Missouri	0.383	0.49	SA	3.66
53	Volta	0.378	0.53	SH	0.05
54	Northern Dvina	0.362	1.11	H	0.01
55	Khatanga	0.357	1.02	H	0.00
56	Irrawaddy	0.353	1.22	H	5.01
57	Indigirka	0.348	0.73	H	0.00
58	Salado (La Pampa)	0.331	0.22	SA	1.73
59	Godavari	0.327	0.63	SH	12.00
60	Salween	0.323	0.93	H	0.74
61	Paranaíba	0.319	0.56	SH	0.10
62	Pechora	0.311	1.24	H	0.00
63	Salado (Atlantic)	0.293	0.56	SH	0.32
64	Dulce	0.293	0.29	SA	1.20
65	Magdalena	0.271	1.36	H	1.48
66	Churchill	0.265	0.79	H	0.00
67	Neva	0.255	1.16	H	0.09
68	Helmand	0.243	0.15	A	3.27
69	Tugai	0.241	0.25	SA	0.03
70	Krishna	0.238	0.47	SA	21.09
71	Ural	0.234	0.40	SA	0.36
72	Fraser	0.227	0.99	H	0.47

ID	River Name	Area (10^6 km^2)	AI	Clim.	Irrig (%)
73	Yana	0.226	0.70	H	0.00
74	RheiN	0.225	1.26	H	1.80
75	Huai He	0.217	0.78	H	31.36
76	Olenek	0.201	0.76	H	0.00
77	Ogooué	0.198	1.10	H	0.00
78	Wisla	0.194	0.85	H	0.39
79	Gairdner	0.193	0.15	A	0.00
80	Anadyr	0.193	0.98	H	0.00
81	Liao	0.192	0.58	SH	14.27
82	Rufiji	0.184	0.65	SH	0.48
83	Kura	0.180	0.54	SH	14.62
84	P'asina	0.167	1.30	H	0.00
85	Chao Phraya	0.166	0.72	H	18.09
86	Hai	0.163	0.47	SA	26.16
87	Taz	0.160	1.32	H	0.00
88	Lake Rudolf	0.160	0.46	SA	0.00
89	Albany	0.156	1.10	H	0.00
90	Koksoak	0.153	1.66	H	0.00
91	Ili	0.153	0.44	SA	2.82
92	Red	0.149	1.12	H	5.16
93	Essequibo	0.148	1.29	H	0.00
94	Cuanza	0.146	0.70	H	0.57
95	Thelon	0.142	0.76	H	0.00
96	Elbe	0.140	0.89	H	1.27
97	Santiago	0.138	0.44	SA	5.62
98	Emba	0.136	0.17	A	0.00
99	Barito	0.136	2.06	H	0.21
100	Fitzroy	0.136	0.41	SA	0.17
101	Mobile	0.135	1.06	H	0.22
102	Sanaga	0.136	1.06	H	0.03
103	Ruvuma	0.133	0.74	H	0.05
104	Swan-Avon	0.128	0.26	SA	0.13
105	Cunene	0.131	0.34	SA	0.14
106	Usumacinta	0.131	1.27	H	0.12
107	Mahanadi	0.127	0.81	H	11.62
108	Burdekin	0.127	0.40	SA	0.15
109	Narmada	0.126	0.65	SH	18.15
110	Brazos	0.125	0.49	SA	6.17

ID	River Name	Area (10^6 km^2)	AI	Clim.	Irrig (%)
111	Tedzen	0.121	0.23	SA	8.97
112	Pur	0.119	1.29	H	0.00
113	Loire	0.118	0.87	H	6.21
114	Kuskokuim	0.118	1.08	H	0.00
115	Kerulen	0.117	0.31	SA	0.03
116	Chubut	0.117	0.26	SA	0.01
117	Flinders	0.117	0.31	SA	0.00
118	Colorado	0.116	0.44	SA	6.71
119	Save	0.116	0.43	SA	0.07
120	Negro	0.115	0.20	SA	2.37
121	Odra	0.115	0.79	H	0.31
122	Mattagami	0.113	1.13	H	0.00
123	Bandama	0.111	0.72	H	0.82
124	Komoe	0.110	0.69	H	0.11
125	Hayes	0.107	0.95	H	0.00
126	Rhone	0.105	1.24	H	4.45
127	Anabar	0.104	0.76	H	0.00
128	Tes-Chem	0.104	0.39	SA	0.50
129	Back	0.103	0.72	H	0.00
130	Severn	0.103	1.08	H	0.00
131	La Grande Riviere	0.102	1.57	H	0.00
132	Neman	0.102	0.95	H	0.24
133	Taimyra	0.101	1.12	H	0.00
134	Broadback	0.100	1.54	H	0.00
135	Tana	0.099	0.38	SA	0.58
136	Saguenay	0.096	1.53	H	0.06
137	Gambia	0.097	0.55	SH	0.01
138	Balsas	0.094	0.58	SH	6.37
139	Doce	0.094	0.82	H	2.14
140	Douro	0.093	0.67	H	5.57
141	Ebro	0.092	0.70	H	9.09
142	Panuco	0.092	0.53	SH	7.44
143	Western Dvina	0.091	1.01	H	0.10
144	Gascoyne	0.090	0.11	A	0.00
145	Garonne	0.089	0.94	H	5.82
146	Churchill	0.088	1.91	H	0.00
147	Tagus Tejo	0.086	0.49	SA	4.95
148	Sacramento	0.085	0.71	H	9.31

ID	River Name	Area (10^6 km^2)	AI	Clim.	Irrig (%)
149	Moore-Hill	0.082	0.22	SA	0.01
150	Sarysu	0.083	0.23	SA	0.01
151	Victoria	0.083	0.37	SA	0.00
152	Fitzroy	0.082	0.28	SA	0.00
153	Seine	0.082	0.85	H	6.54
154	Mezen	0.081	1.15	H	0.00
155	Ashburton	0.079	0.13	A	0.00
156	San Joaquin	0.079	0.43	SA	13.93
157	Rio Colorado	0.078	0.22	SA	0.37
158	Guadiana	0.077	0.43	SA	9.40
159	Penzina	0.077	1.04	H	0.00
160	Susquehana	0.075	1.03	H	0.38
161	Mamberamo	0.074	2.05	H	0.00
162	Sepik	0.074	1.98	H	0.00
163	Mearim	0.074	0.78	H	0.06
164	Kuban	0.074	2.06	H	0.00
165	Fly	0.074	0.86	H	0.10
166	Sassandra	0.072	1.39	H	0.00
167	Nottaway	0.071	0.55	SH	0.00

ID	River Name	Area (10^6 km^2)	AI	Clim.	Irrig (%)
168	Mitchell	0.069	1.30	H	0.00
169	Nadym	0.069	1.02	H	1.04
170	Paraiba	0.068	1.10	H	0.00
171	Attawapiskat	0.066	0.14	A	0.00
172	Murchison	0.065	1.10	H	2.08
173	Yalu	0.063	0.98	H	4.59
174	Apalachicola	0.061	0.85	H	2.44
175	Po	0.061	1.42	H	24.04
176	Lurio	0.060	0.57	SH	0.00
177	Alazeja	0.059	0.53	SH	0.00
178	Guadalquivir	0.059	0.42	SA	12.33
179	Chu	0.058	1.08	H	3.99
180	Kemi	0.057	0.50	SA	1.72
181	Sakarya	0.057	1.20	H	0.00
182	Fortescue	0.057	0.18	A	0.00
183	Onega	0.052	1.15	H	0.01
184	Saint John	0.051	1.39	H	0.15
185	Skeena	0.050	1.40	H	0.01
186	Narva	0.047	1.04	H	0.02

Table S4. (a). **Decreasing TWSA trends** (Apr. 2002 – Dec. 2014) **(basin wide mean: mm/yr)** for selected basins ranked according to GRACE CSR mascons (CSR-M) and corresponding trends for GHWRMs (WGHM, WGHM no human intervention [NHI], PCR-GLOBWB and PCR-GLOBWB-NHI) and LSMs (GLDAS-1.0 MOSAIC, VIC, and GLDAS-2.1 NOAH-3.3 and CLSMF2.5, and CLM-4.0).

River	Area 10^6 km^2	AI	Climate	AEI %	Irr. GW %	Irr. SW %	GRACE				GHWRMs				Land Surface Models				
							CSR-M	JPLMdsf	CSRT-GSH.sf	Uncert mm/yr	WGHM	WGHM-NHI	PCR-GLOBWB	PCR-NHI	MOSAIC	VIC	NOAH-3.3	CLSM-F2.5	CLM-4.0
Rio Colorado	0.08	0.22	SA	0.37	0.00	0.00	-15.24	-15.78	-11.23	0.85	-2.42	-1.19	-2.89	-2.26	-1.98	-1.58	-4.48	-3.19	-9.20
Thelon	0.14	0.76	H	0.00	0.00	0.00	-15.24	-12.65	-14.45	0.62	-15.32	-15.32	-1.77	-1.76	-13.63	-15.96	-10.88	-12.55	-2.08
Brahmaputra	0.66	1.19	H	6.55	3.84	1.93	-14.53	-13.49	-11.09	0.59	-1.91	-1.83	-3.89	-3.94	3.09	-1.44	-3.12	-5.79	-2.80
Kura	0.18	0.54	SH	14.62	1.07	9.40	-13.95	-13.02	-14.36	0.82	-3.42	-1.52	-7.99	-3.18	-10.38	-2.28	-2.99	-7.10	-2.45
Euphrates	0.76	0.27	SA	10.15	1.77	5.57	-13.92	-15.81	-19.41	0.82	-4.71	-1.23	-4.73	-0.88	-3.81	-1.28	-3.97	-1.86	-8.09
Brazos	0.13	0.49	SA	6.17	5.69	0.48	-12.79	-18.83	-12.31	1.04	-24.58	-3.72	-18.11	-1.49	-9.54	-3.45	-9.16	-10.52	-21.82
Ganges	1.03	0.73	H	30.62	20.44	9.53	-11.80	-16.90	-12.03	1.00	-6.39	0.38	4.61	15.43	-3.57	-5.17	0.59	-2.78	7.19
Rio Grande	0.14	0.17	A	0.00	0.00	0.00	-10.80	-19.60	-15.24	0.55	-0.03	-0.01	-0.89	-0.91	-4.16	-0.63	-5.09	-2.61	-4.66
Don	0.42	0.62	SH	1.50	0.14	0.55	-10.30	-14.01	-14.56	1.02	-2.82	-2.56	-1.49	-1.31	-12.69	-4.12	-6.84	-12.76	-8.24
Colorado	0.12	0.44	SA	6.71	6.05	0.63	-10.25	-18.06	-16.67	1.14	-24.01	-4.78	-15.44	-1.02	-8.20	-2.88	-11.05	-8.70	-17.72
De Grey	0.47	0.14	A	0.00	0.00	0.00	-8.41	-10.40	-6.08	0.92	-0.01	-0.01	-0.37	-0.37	0.81	0.21	-0.96	-0.47	-7.92
Indus	0.97	0.39	SA	22.71	8.41	12.76	-8.32	-10.27	-7.81	0.59	-3.21	1.23	-39.55	5.82	-4.88	-8.88	3.33	1.11	5.93
Arkansas	0.67	0.61	SH	3.78	4.17	0.67	-8.10	-10.83	-8.35	0.91	-14.35	-1.51	-9.12	-0.27	-8.10	-2.12	-5.82	-6.48	-7.72
Sao Francisco	0.61	0.55	SH	1.03	0.38	0.48	-7.90	-11.42	-8.29	1.33	-4.31	-4.74	-2.18	-1.99	-3.14	-0.66	-3.05	-4.31	-10.28
Hai	0.16	0.47	SA	26.16	17.86	6.03	-7.65	-11.18	-5.97	0.59	-25.01	0.69	-34.68	2.49	0.67	1.09	-0.89	0.06	-2.24
Ural	0.23	0.40	SA	0.36	0.03	0.12	-7.43	-10.78	-8.30	0.60	-0.06	0.36	-2.18	-2.03	-7.26	-2.38	-5.49	-8.10	-8.46
Doce	0.09	0.82	H	2.14	0.21	1.89	-7.08	-14.01	-2.27	1.88	-2.24	-2.20	13.71	13.85	1.82	3.01	-3.87	-6.13	-5.67
Syr Darya	0.42	0.29	SA	7.90	0.38	6.31	-5.34	-6.54	-4.83	0.54	-2.85	-1.03	-3.35	-1.79	-5.86	-4.35	-3.67	-3.07	-5.09
Huaihe	0.22	0.78	H	31.36	9.87	20.40	-4.91	-8.05	-5.01	0.95	-7.46	-3.22	-12.38	-6.04	-23.68	-10.44	-4.26	-6.97	-16.69
Huanghe	0.79	0.52	SH	9.19	3.48	3.99	-4.89	-5.88	-5.85	0.48	0.92	0.77	-4.17	0.37	-0.74	-0.65	-1.49	-2.33	0.00
Volga	1.41	0.89	H	0.50	0.09	0.34	-4.58	-4.99	-6.07	0.70	-0.38	0.40	-1.98	-1.82	-18.99	-4.01	-4.01	-11.35	-3.14
Amu Darya	0.49	0.54	SH	8.92	0.22	5.02	-4.37	-4.24	-5.04	0.74	0.11	0.59	13.03	13.68	-8.70	-6.04	-1.23	-1.77	-0.77
Dnieper	0.51	0.78	H	2.69	0.02	2.12	-4.05	-5.49	-6.65	0.76	1.13	0.98	-1.09	-1.29	-10.43	-2.69	-3.63	-4.72	0.83
San Joaquin	0.08	0.43	SA	13.93	8.46	5.44	-3.68	-7.45	1.04	1.66	-9.75	-0.99	-31.78	-4.07	-1.65	-3.00	-4.69	-4.26	-8.61
Rio Grande	0.62	0.26	SA	1.91	0.60	0.88	-3.65	-5.70	-4.32	0.47	-2.57	-0.58	-3.16	-1.09	-3.21	-0.81	-4.62	-5.07	-5.69

CSRT-GSH: GRACE CSR Tellus Gridded Spherical Harmonic solution, sf, rescaled, CSR-M, mascons, dsf, downscaled from 3˚ to 0.5˚;

GRACE uncertainty includes uncertainty among 3 GRACE solutions, trend (slope) uncertainty in solutions, and GIA uncertainty (SI, Section 4.2).

Table S4 (b). **Increasing TWSA trends** (Apr. 2002 – Dec. 2014) **(basin wide mean: mm/yr)** for selected basins ranked according to GRACE CSR mascons (CSR-M) and corresponding trends for GHWRMs (WGHM, WGHM no human intervention [NHI], PCR-GLOBWB and PCR-GLOBWB-NHI) and LSMs (GLDAS-1.0 MOSAIC, VIC, and GLDAS-2.1 NOAH-3.3 and CLSMF2.5, and CLM-4.0).

River Units (mm/yr)	*Area 10^6 km^2*	*AI*	*Climate*	*AEI %*	*Irr. GW %*	*Irr. SW %*	*GRACE*				*GHWRMs*				*Land Surface Models*				
							CSR-M	*JPL-M.dsf*	*CSRT-GSH.sf*	*Trend Uncert.*	*WGHM*	*WGHM-NHI*	*PCR-GLOBWB*	*PCR-NHI*	*NOAH-3.3*	*MOSAIC*	*VIC*	*CLSM-F2.5*	*.CLM-4.0*
Fitzroy	0.14	0.41	SA	0.17	0.01	0.07	15.39	10.93	11.14	0.94	2.17	1.73	8.73	8.26	8.41	-0.35	0.60	2.45	25.85
Broadback	0.10	1.54	H	0.00	0.00	0.00	14.55	16.42	13.66	0.69	0.06	0.06	-2.95	-2.95	-3.44	-35.66	-28.52	-38.82	1.05
Okavango	0.79	0.29	SA	0.02	0.00	0.00	14.55	16.60	10.36	0.68	1.59	1.59	0.08	0.09	1.37	2.31	1.24	-1.53	1.27
Saguenay	0.10	1.53	H	0.06	0.01	0.01	14.27	16.74	14.67	0.74	0.82	-0.49	-1.94	-2.04	-4.38	-33.13	-17.38	-29.90	-0.76
Cunene	0.13	0.34	SA	0.14	0.00	0.00	13.30	25.02	32.86	1.29	2.57	2.04	-0.12	-0.11	-4.90	5.99	5.49	-3.49	-1.45
VOLTA	0.38	0.53	SH	0.05	0.00	0.02	12.09	12.47	10.11	0.79	-2.63	-1.81	4.20	3.43	-2.25	0.64	1.53	-6.93	18.17
Essequibo	0.15	1.29	H	0.00	0.00	0.00	11.57	14.72	11.39	2.00	-5.78	-5.78	-19.82	-19.84	-3.79	-48.67	-10.12	-23.49	3.69
Zambezi	1.34	0.55	SH	0.30	0.00	0.05	10.24	12.13	10.68	1.01	2.38	0.59	-1.26	-1.54	-0.76	-2.28	-0.38	-3.62	1.74
Burdekin	0.13	0.40	SA	0.15	0.00	0.00	9.68	16.72	10.15	1.06	1.69	1.74	27.60	27.61	5.86	2.08	0.16	1.40	39.42
Koksoak	0.15	1.66	H	0.00	0.00	0.00	8.04	19.07	11.04	0.66	-1.02	-2.06	-4.03	-2.36	-6.91	-20.25	-28.97	-16.92	-2.28
Columbia	0.72	0.78	H	3.98	0.88	2.26	7.95	7.55	8.93	0.62	1.76	1.24	1.89	1.92	-3.00	5.11	1.69	-2.51	-0.34
Godavari	0.33	0.63	SH	12.00	6.72	3.49	7.82	9.80	6.80	1.12	-4.19	0.31	59.11	49.33	-0.77	-5.18	-2.33	-1.19	25.08
Gambia	0.10	0.55	SH	0.01	0.00	0.00	7.70	15.03	10.64	0.99	0.80	0.77	6.22	6.16	-0.03	5.43	5.32	0.01	22.49
La Grande Riviere	0.10	1.57	H	0.00	0.00	0.00	7.55	20.22	12.44	0.69	-18.47	-9.60	-4.60	-2.84	-2.28	-24.11	-23.89	-21.96	-2.17
Orinoco	0.91	1.34	H	0.94	0.05	0.39	7.32	5.15	4.66	1.41	-5.97	-4.25	-27.14	-25.81	-3.29	-3.55	-1.69	-11.75	-8.76
Amazon	6.23	1.25	H	0.15	0.02	0.09	6.94	6.99	6.59	0.87	1.73	1.70	-10.67	-10.62	-0.19	-11.35	-2.97	-5.11	-0.55
Krishna	0.24	0.47	SA	21.09	10.99	9.85	6.81	6.08	6.71	1.27	-2.68	1.25	55.39	35.65	-2.25	-4.88	-1.59	-1.10	44.79
Lake Rudolf	0.16	0.46	SA	0.00	0.00	0.00	6.38	10.34	3.51	0.63	3.44	3.28	4.68	4.72	-2.60	3.87	2.87	-1.89	7.66
Murray	1.07	0.36	SA	2.46	0.30	1.48	5.26	8.66	8.10	0.92	3.78	3.03	2.26	2.11	5.52	2.69	2.76	1.63	-4.58
Kolyma	0.64	0.75	H	0.00	0.00	0.00	5.09	3.11	4.14	0.55	5.16	5.16	2.85	2.91	4.14	-6.73	-0.89	4.67	7.87
Niger	2.12	0.34	SA	0.18	0.00	0.02	4.59	5.54	5.18	0.32	2.28	1.93	-0.70	-0.83	-0.23	-1.46	0.42	-4.53	0.49
Amur	1.87	0.83	H	2.04	0.99	0.72	4.36	4.23	4.59	0.69	2.58	2.72	6.10	6.39	1.25	-3.08	4.15	1.25	0.96
Senegal	0.44	0.28	SA	0.32	0.02	0.20	3.79	5.80	5.59	0.51	2.14	1.82	0.89	1.16	-0.20	4.84	4.55	-0.32	8.21
Anadyr	0.19	0.98	H	0.00	0.00	0.00	3.66	3.71	3.70	0.83	-1.42	-1.42	1.57	1.57	3.52	-1.98	-0.96	4.50	6.49
Juba	0.74	0.26	SA	0.17	0.00	0.05	3.22	1.04	3.90	0.45	0.58	0.58	-0.18	-0.19	-2.35	-0.65	0.63	-1.04	-1.49
Orange	1.00	0.22	SA	0.63	0.03	0.30	2.99	5.36	2.64	0.35	0.48	0.26	0.11	0.09	-0.75	-2.10	-0.32	-0.97	-2.45
Mississippi	3.25	0.68	H	3.92	3.09	0.76	2.91	2.07	-0.58	0.69	-2.79	1.30	1.39	1.67	-2.15	-5.40	-0.62	-3.70	2.54
Yangtze	1.83	1.01	H	8.40	0.34	7.70	2.83	4.80	1.57	0.55	0.54	0.75	2.01	0.33	-1.51	-2.98	-0.61	-3.44	0.31
Magdalena	0.27	1.36	H	1.48	0.06	1.07	2.74	-0.62	0.20	1.30	4.20	3.84	61.83	61.55	-1.29	4.04	-5.27	-11.11	5.29
Parana	2.99	0.76	H	0.87	0.18	0.53	2.67	3.60	0.52	0.77	-0.52	-0.95	4.02	3.74	1.41	-4.25	-2.11	1.42	-4.06
Missouri	1.38	0.49	SA	3.66	2.93	1.16	2.45	2.56	1.06	0.73	1.15	1.10	0.34	1.68	0.07	0.35	0.49	-0.23	2.07
St. Lawrence	1.11	1.10	H	0.48	0.26	0.14	2.41	1.70	2.51	0.68	-3.06	-4.48	8.23	8.58	-1.36	-15.54	-4.93	-4.49	2.40

Table S5a. **Uncertainty** in GRACE TWSA trends for increasing TWSA trends ranked based on GRACE CSR-M for selected basins, including uncertainty from variability in trends among the three GRACE solutions (solution uncertainty: standard deviation from trends in CSR-M, JPL-M.dsf and CSRT-GSH.sf), trend uncertainty based on uncertainty in regression slopes from the three solutions, and glacial Isostatic Adjustment (GIA) uncertainty based on standard deviation from four models. The combined uncertainty is the square root of the sum of the squares of the solution, trend, and GIA uncertainties.

ID	*River*	*Area 10^6 km^2*	*CSR-M*	*JPL-M.dsf*	*CSRT-GSH.sf*	*Solution Uncertainty*	*CSR-M*	*JPL-M.dsf*	*CSRT-GSH.sf*	*Trend Uncertainty*	*GIA Uncertainty*	*Combined Uncertainty*
Decreasing TWSA Trends (km^3/yr)												
19	Ganges	1.03	-12.2	-17.4	-12.4	3.0	0.9	1.2	1.0	0.12	0.06	3.0
30	Euphrates	0.76	-10.6	-12.0	-14.8	2.1	0.5	0.6	0.6	0.08	0.02	2.1
34	Brahmaputra	0.66	-9.5	-8.9	-7.3	1.2	0.4	0.5	0.4	0.03	0.05	1.2
21	Indus	0.97	-8.1	-10.0	-7.6	1.3	0.5	0.6	0.6	0.05	0.06	1.3
13	Volga	1.41	-6.4	-7.0	-8.5	1.1	0.9	1.1	1.0	0.12	0.19	1.1
33	Arkansas	0.67	-5.4	-7.2	-5.6	1.0	0.6	0.7	0.6	0.05	0.12	1.0
38	Sao Francisco	0.61	-4.8	-7.0	-5.1	1.2	0.8	0.9	0.8	0.06	0.09	1.2
47	Don	0.42	-4.4	-6.0	-6.2	1.0	0.4	0.4	0.5	0.06	0.04	1.0
29	Huanghe	0.79	-3.8	-4.6	-4.6	0.4	0.3	0.4	0.4	0.06	0.07	0.5
3	Ob	3.00	-3.6	-3.8	-4.3	0.4	1.6	1.9	1.8	0.12	0.19	0.4
11	Tamanrasett	1.76	-2.6	-2.4	-2.0	0.3	0.2	0.3	0.2	0.05	0.13	0.4
37	Rio Grande	0.62	-2.2	-3.5	-2.7	0.6	0.3	0.4	0.2	0.07	0.08	0.6
48	Syr Darya	0.42	-2.2	-2.7	-2.0	0.4	0.2	0.2	0.3	0.03	0.04	0.4
90	Thelon	0.14	-2.2	-1.8	-2.1	0.2	0.1	0.1	0.1	0.01	0.63	0.7
42	Amu Darya	0.49	-2.1	-2.1	-2.5	0.2	0.3	0.4	0.3	0.06	0.04	0.2
12	MacKenzie	1.74	-1.9	-0.4	-3.2	1.4	0.5	0.6	0.6	0.07	1.13	1.8
105	Brazos	0.13	-1.6	-2.4	-1.5	0.5	0.1	0.2	0.1	0.02	0.04	0.5
81	Hai	0.16	-1.2	-1.8	-1.0	0.4	0.1	0.1	0.1	0.01	0.03	0.4
113	Colorado	0.12	-1.2	-2.1	-1.9	0.5	0.1	0.1	0.1	0.02	0.03	0.5
70	Huaihe	0.22	-1.1	-1.8	-1.1	0.4	0.2	0.2	0.2	0.02	0.03	0.4
46	Tarim	0.44	-0.9	-0.9	0.6	0.9	0.1	0.2	0.1	0.03	0.05	0.9

Table 5b. **Uncertainty** in GRACE TWSA trends for decreasing TWSA trends ranked based on GRACE CSR-M for selected basins, including uncertainty from variability in trends among the three GRACE solutions (solution uncertainty: standard deviation from trends in CSR-M, JPL-M.dsf and CSRT-GSH.sf), trend uncertainty based on uncertainty in regression slopes from the three solutions, and glacial Isostatic Adjustment (GIA) uncertainty based on standard deviation from four models. The combined uncertainty is the square root of the sum of the squares of the solution, trend, and GIA uncertainties.

ID	*River*	*Area 10^6 Km^2*	*CSR-M*	*JPL-M.dsf*	*CSRT-GSH.sf*	*Solution Uncertainty*	*CSR-M*	*JPL-M.dsf*	*CSRT-GSH.sf*	*Trend Uncertainty*	*GIA Uncertainty*	*Combined Uncertainty*
Decreasing TWSA Trends (km^3/yr)												
1	Amazon	6.23	43.2	43.6	41.1	1.3	4.9	5.4	6.0	0.55	0.33	1.5
14	Zambezi	1.34	13.7	16.3	14.3	1.3	1.2	1.5	1.4	0.13	0.10	1.3
27	Okovango	0.79	11.5	13.2	8.2	2.5	0.6	0.6	0.4	0.08	0.08	2.5
8	Niger	2.12	9.8	11.8	11.0	1.0	0.6	0.7	0.7	0.07	0.17	1.0
2	Mississippi	3.25	9.5	6.7	-1.9	5.9	2.0	2.3	2.4	0.23	0.48	6.0
9	Amur	1.87	8.1	7.9	8.6	0.3	1.1	1.3	1.5	0.20	0.11	0.4
4	Parana	2.99	8.0	10.8	1.5	4.7	2.1	2.3	2.5	0.20	0.11	4.7
23	Orinoco	0.91	6.7	4.7	4.3	1.3	1.2	1.2	1.4	0.11	0.16	1.3
32	Columbia	0.72	5.7	5.4	6.4	0.5	0.3	0.6	0.4	0.12	0.15	0.5
18	Murray	1.07	5.6	9.3	8.7	2.0	0.9	1.1	1.0	0.12	0.12	2.0
10	Yangtze	1.83	5.2	8.8	2.9	3.0	0.8	1.0	1.2	0.22	0.09	3.0
50	Volta	0.38	4.6	4.7	3.8	0.5	0.3	0.4	0.2	0.07	0.08	0.5
5	Nile	2.98	4.1	14.0	-3.8	8.9	1.1	1.6	1.7	0.32	0.09	8.9
6	Yenisei	2.61	3.7	4.6	4.0	0.5	1.1	1.1	1.4	0.15	0.19	0.5
	Missouri	1.38	3.4	3.5	1.5	0.1	1.0	0.0	0.9	0.09	0.34	0.4
35	Kolyma	0.64	3.3	2.0	2.6	0.6	0.3	0.4	0.4	0.04	0.13	0.6
20	Orange	1.00	3.0	5.4	2.6	1.5	0.3	0.4	0.3	0.03	0.08	1.5
17	St. Lawrence	1.11	2.7	1.9	2.8	0.5	0.8	0.9	0.7	0.07	0.47	0.7
7	Lena	2.35	2.7	-2.0	-0.8	2.4	1.1	1.3	1.4	0.13	0.21	2.4
55	Godavari	0.33	2.6	3.2	2.2	0.5	0.3	0.4	0.4	0.04	0.03	0.5

Table S6a. Linear regression statistics comparing GRACE TWSA trends to each other considering large declining and rising TWSA trends based on CSR-M data. Statistics include the slope (b), intercept (c) and coefficient of determination (r^2). GRACE solutions include CSR mascons (CSR-M), JPL-M, and CSR Tellus, gridded spherical harmonic solutions rescaled. Subscript sf refers to scaling factors and dsf refers to downscaled.

	CSR-M			*CSRT-GSH.sf*			*JPL-M.dsf*		
	b	*c*	*r^2*	*b*	*c*	*r^2*	*b*	*c*	*r^2*
CSRM				0.97	0.45	0.90	0.86	0.06	0.94
CSRT-GSH.sf	0.93	-0.38	0.90				0.80	-0.32	0.85
JPL-M.dsf	1.09	-0.02	0.94	1.05	0.48	0.85			

Table S6b. Linear regression statistics comparing modeled TWSA trends to trends from GRACE solutions considering large declining and rising TWSA trends based on CSR-M data (94 basins). Statistics include the slope (b), intercept (c) and coefficient of determination (r^2). GRACE solutions include CSR mascons (CSR-M), JPL-M, and CSR Tellus, gridded spherical harmonic solutions. Subscript sf refers to scaling factors and dsf refers to downscaled. Models include GHWRMs WGHM and PCR-GLOBWB and land surface models (MOSAIC, VIC, NOAH-3.3, CLSM-F2.5, and CLM-4.0).

	GRACE CSR-M			*GRACE CSRT-GSH.sf*			*GRACE JPL-M.dsf*		
	b	*c*	*r^2*	*b*	*c*	*r^2*	*b*	*c*	*r^2*
WGHM	0.24	-0.30	0.28	0.28	-0.21	0.36	0.24	-0.32	0.35
PCR-GLOBWB	-0.64	-0.02	0.17	-0.66	-0.29	0.17	-0.46	-0.13	0.11
MOSAIC	-0.85	-3.12	0.24	-0.72	-3.55	0.17	-0.63	-3.26	0.17
VIC	-0.16	-1.00	0.07	-0.12	-1.09	0.04	-0.10	-1.05	0.03
NOAH-3.3	0.02	-0.97	0.00	0.07	-0.98	0.02	0.02	-0.98	0.00
CLSM-F2.5	-0.39	-2.27	0.22	-0.32	-2.47	0.14	-0.30	-2.33	0.17
CLM-4.0	0.05	0.04	0.00	0.05	0.06	0.00	0.03	0.05	0.00

Table S7. Results of Kruskal Wallis test (74) applied to TWSA trends with basins in the zone of (a) decreasing and (b) increasing CSR-M trends. The null hypothesis is that the TWSA trends from different GRACE solutions and models belong to the same population. Values of KW statistic (upper row) and associated P values (lower row) are tabulated. P values exceeding 0.05 are considered statistically significant, indicating that the TWSA trends are from the same population. P values ≥0.05 are shown in bold.

7a) Decreasing TWSA trends

	CSRT-GSH	*JPL-M.dsf*	*WGHM*	*PCR-GLOBWB*	*MOSAIC*	*VIC*	*NOAH-3.3*	*CLM-4.0*	*CLSM*
CSR-M	0.04	1.93	21.66	10.95	2.78	21.31	12.93	3.82	5.76
	0.84	**0.17**	0.00	0.00	**0.10**	0.00	0.00	**0.05**	0.02
CSRT-GSH.sf		0.79	18.16	9.82	3.09	18.61	11.15	3.01	5.76
		0.37	0.00	0.00	**0.08**	0.00	0.00	**0.08**	0.02
JPL-M.dsf			25.86	15.85	5.58	25.86	18.03	6.59	10.60
			0.00	0.00	0.02	0.00	0.00	0.01	0.00
WGHM				1.99	4.12	**0.06**	1.95	6.87	5.41
				0.16	0.04	**0.81**	**0.16**	0.01	0.02
PCR-GLOBWB					1.19	2.25	0.00	2.03	0.74
					0.27	**0.13**	**0.99**	**0.15**	**0.39**
MOSAIC						4.56	1.53	0.00	0.15
						0.03	**0.22**	**0.95**	**0.70**
VIC							2.21	6.44	5.55
							0.14	0.01	0.02
NOAH-3.3								2.08	0.89
								0.15	**0.35**
CLM-4.0									0.32
									0.57

7b) Increasing TWSA trends

	CSRT-GSH.sf	*JPL-M.dfs*	*WGHM-Hai*	*PCR-NonNat*	*MOSAIC*	*VIC*	*NOAH-3.3*	*CLM-4.0*	*CLSM*
CSR-M	1.07	0.81	24.79	11.96	51.92	48.28	48.90	8.27	57.22
	0.30	**0.37**	0.00	0.00	0.00	0.00	0.00	0.00	0.00
CSRT GSH		3.52	14.70	5.71	41.12	34.40	34.80	3.79	45.47
		0.06	0.00	0.02	0.00	0.00	0.00	**0.05**	0.00
JPL-M.dfs			25.55	13.00	50.97	45.89	46.45	10.91	55.70
			0.00	0.00	0.00	0.00	0.00	0.00	0.00
WGHM-Hai				1.34	15.94	5.55	7.82	2.57	20.50
				0.25	0.00	0.02	0.01	**0.11**	0.00
PCR-NonNat					20.43	9.91	12.10	0.14	24.55
					0.00	0.00	0.00	**0.71**	0.00
MOSAIC						4.41	4.12	21.76	0.00
						0.04	0.04	0.00	**0.95**
VIC							0.06	13.31	5.88
							0.80	0.00	0.02
NOAH-3.3								14.81	5.06
								0.00	0.02
CLM-4.0									26.21
									0.00

Table S8. Linear regression parameters (b is slope, c is intercept, and r^2 is coefficient of determination) for relationships between modeled TWSA trends, including 181 basins (Congo, Serrado, Yukon and Missouri basins excluded). Models include GHWRMs (WGHM, PCR-GLOBWB) and LSMs (GLDAS-1.0 MOSAIC, and VIC and GLDAS- 2.1 NOAH3.3 and CLSMF2.5, and CLM-4.0).

Trend km^3/yr	*GHWRMs*						*Land Surface Models*														
	b	*c*	*r^2*	*b*	*c*	*r^2*	*b*	*c*	*r^2*	*b*	*c*	*r^2*	*b*	*c*	*r^2*	*b*	*c*	*r^2*	*b*	*c*	*r^2*
	WGHM			*PCR-GLOBWB*			*MOSAIC*			*VIC*			*NOAH-3.3*			*CLSM-F2.5*			*CLM-4.0*		
WGHM				-0.04	-0.01	0.01	-0.05	-0.14	0.04	0.09	0.07	0.02	0.02	0.02	0.00	-0.12	-0.23	0.08	0.11	0.01	0.03
PCR-GLOBWB	-0.39	-0.25	0.01				0.39	0.78	0.21	1.11	0.57	0.21	0.13	-0.17	0.00	0.54	0.79	0.15	0.40	-0.22	0.03
GLDAS-1.0 MOSAIC	-0.76	-2.64	0.04	0.55	-2.51	0.21				2.14	-1.06	0.55	1.65	-1.57	0.23	1.32	-0.09	0.65	0.19	-2.63	0.01
GLDAS-1.0 VIC	0.16	-0.74	0.02	0.19	-0.69	0.21	0.26	-0.06	0.55				0.45	-0.44	0.14	0.27	-0.21	0.23	0.07	-0.73	0.01
GLDAS-2.1 NOAH-3.3	0.03	-0.65	0.00	0.01	-0.64	0.00	0.14	-0.28	0.23	0.32	-0.41	0.14				0.33	-0.01	0.49	-0.07	-0.65	0.01
GLDAS-2.1 CLSM-F2.5	-0.66	-1.93	0.08	0.28	-1.86	0.15	0.49	-0.63	0.65	0.84	-1.31	0.23	1.47	-0.98	0.49				-0.07	-1.94	0.00
CLM-4.0	0.25	-0.06	0.03	0.09	-0.04	0.03	0.03	0.02	0.01	0.09	0.01	0.01	-0.13	-0.15	0.01	-0.03	-0.12	0.00			

Table S9. Spearman's rho coefficient (ρ) between TWSA from CSR-M and GLDAS 2.1 precipitation from NOAH-3.3 model with no time lag and maximum value of ρ and associated time lag in months.

River Basin	ρ	*Max.* ρ	*Lag (mo.)*
AMAZON	0.57	0.57	0
AMUR	-0.06	0.52	-5
Arkansas	0.23	0.53	-5
BRAHMAPUTRA	0.65	0.79	-1
BRAZOS	0.39	0.51	-5
COLUMBIA	0.50	0.50	0
DON	0.49	0.49	0
EUPHRATES	0.74	0.74	0
GANGES	0.90	0.90	0
HAI	0.28	0.38	-9
HUAIHE	0.57	0.57	0
HUANGHE	0.57	0.57	0
INDUS	0.32	0.42	-4
KOLYMA	-0.21	0.58	-7
LENA	-0.65	0.56	-7
MACKENZIE	-0.68	0.64	-6
MISSISSIPPI	0.04	0.62	-5
Missouri	0.21	0.68	-4
MURRAY	0.51	0.60	-7
NILE	0.80	0.80	0
OB	-0.02	0.53	-7
Okavango	0.50	0.50	0
ORINOCO	0.82	0.82	-1
VOLGA	0.23	0.32	-9
Yenisei	-0.61	0.75	-7
YUKON	-0.22	0.58	-8
Zambezi	0.67	0.67	0
Yangtze	0.45	0.55	-1

Table S10. Median, mean, 10th and 90th percentiles, and standard deviation (Std. dev.) in TWSA trends for corresponding values to GRACE CSR-M large decreasing and increasing trends (≤ 0.5 km^3/yr and ≥0.5 km^3/yr) and CSR-M mid-range (±0.5 km^3/yr) including other GRACE solutions (JPL-M and CSRT-GSH.sf) and GHWRMs (WGHM and PCR-GLOBWB with human intervention and without human intervention, NHI), and LSMs (MOSAIC, VIC, NOAH3.3, CLSMF2.5, and CLM-4.0). The number of basins in each group is listed: (45 basins with CSR-M trends ≤-0.5 km^3/yr (decreasing trends); 49 basins in the mid-range ±0.5 km3/yr and 87 basins with trends ≥0.5 km^3/yr (increasing trends)). The number of basins totals 181, excluding the Yukon Basin (glacier leakage), Salado basins (glacier leakage and earthquake), Congo Basin (trend not significant), and Missouri Basin (included in Mississippi basin).

	GRACE			*GHWRMs*				*Land Surface Models*				
	CSR-M	*JPL-M.dsf*	*CSRT-GSH*	*WGHM*	*WGHM-NHI*	*PCR-GLOBWB*	*PCR-NHI*	*MOSAIC*	*VIC*	*NOAH 3.3*	*CLSM-F2.5*	*CLM-4.0*
CSR-M TWSA trends ≤-0.5 km^3/yr (45 basins)												
Median	-1.47	-2.18	-1.94	-0.31	-0.09	-0.67	-0.34	-1.07	-0.40	-0.82	-1.09	-1.36
Mean	-2.61	-3.23	-2.78	-1.02	-0.14	-1.81	0.11	-2.99	-1.06	-1.24	-2.22	-1.60
10 - 90 Pi	5.35	6.46	6.48	3.43	1.60	3.67	2.62	6.17	4.76	3.81	4.12	6.06
Std. dev.	2.78	3.45	3.18	2.05	0.84	5.97	2.98	8.58	2.68	2.31	3.79	2.85
CSR-M TWSA trends within ±0.5 km^3/yr (49 basins)												
Median	-0.02	0.01	-0.08	0.04	0.04	0.05	0.07	-0.31	-0.06	-0.09	-0.25	0.02
Mean	-0.03	0.05	-0.10	0.00	0.07	0.01	0.09	-0.98	-0.42	-0.18	-0.85	-0.19
10 - 90 Pi	0.60	1.20	1.17	0.93	0.76	2.36	2.05	3.29	1.79	1.03	2.65	1.55
Std. dev.	0.23	0.50	0.64	0.56	0.37	1.43	1.29	2.31	1.08	0.50	2.00	0.80
CSR-M TWSA trends ≥0.5 km^3/yr (87 basins)												
Median	1.74	2.13	1.59	0.22	0.26	0.60	0.59	-1.57	-0.19	-0.42	-0.97	1.04
Mean	3.90	4.56	3.23	0.68	0.90	0.62	0.46	-4.65	-1.23	-0.73	-2.97	1.56
10 - 90 Pi	7.67	10.29	8.00	5.84	5.01	13.05	11.18	15.47	6.39	4.19	10.81	9.71
Std. dev.	6.53	4.56	3.23	0.68	0.90	0.62	0.46	-4.65	-1.23	-0.73	-2.97	1.56

Table S11. Median TWSA trends in GRACE and models in basins with large rising CSR-M trends (≥0.5 km^3/yr) and large declining CSR-M trends (≤-0.5 km^3/yr).

GRACE CSR-M Ranked TWSA trends	*# basins*	*GRACE*				*GHWRMs*				*Land Surface Models*				
		CSR-M	*JPL-M.dsf*	*CSRT-GSH.sf*	*Uncertainty*	*WGHM*	*WGHM-NHI*	*PCR-GLOBWB*	*PCR NHI*	*MOSAIC*	*VIC*	*NOAH-3.3*	*CLSM-F2.5*	*CLM-4.0*
Global Net TWSA Trends (km^3/yr)														
Sum	181	71	82	25	15.6	-12	44	-50	36	-448	-144	-107	-320	-13
≤-0.5 km^3/yr	45	-118	-145	-125	6.2	-46	-6.2	-82	5.1	-134	-48	-56	-100	-72
≥0.5 km^3/yr	49	191	224	158	13.8	33	44	31	22	-228	-60	-36	-146	76
Sum Inc + Dec	94	73	78	33	15.0	-12	38	-51	27	-362	-108	-91	-245	4.3
Contribution to Global Mean Sea Level (mm/yr)														
Total	181	-0.20	-0.23	-0.07	0.09	0.03	-0.12	0.14	-0.10	1.24	0.40	0.30	0.89	0.04
Human int.						0.15		0.24						

Net TWSA trends (km^3/yr) were calculated by summing TWSA trends for GRACE solutions and global models, over all 181 basins (excluding Congo Basin, two Serrado basins, Yukon, and Missouri basins). The contribution of net TWSA trends on global mean sea level (GMSL) was calculated by dividing the TWSA trend by the ocean area ($361x10^6$ km^2) and changing the sign. GRACE solutions include (CSR-M, JPL-M, CSR Tellus gridded spherical harmonics [CSRT-GSH]). Models include global hydrological and water resource models (GHWRMs, WGHM and PCR-GLOBWB) and land surface models (MOSAIC, VIC, NOAH-3.3, CLSM-F2.5, and CLM-4.0). Uncertainty in the GRACE contribution to GMSL also includes geocenter uncertainty (0.05 mm/yr) (67). Human intervention was estimated by comparing WGHM and WGHM-NHI (no human intervention) and PCR-GLOBWB and PCR-GLOBWB-NHI. Human intervention is -56 km^3/yr (-12-44 km^3/yr = -56 km^3/yr) for WGHM, dividing by ocean area ($361x10^6$ km^2) and changing sign results in 0.15 mm/yr.

Table S12. Data corresponding to Fig. S14 showing trend contributions to global mean sea level from this study and other studies based on similar time periods (2002 – 2014). The GRACE data include human and climate impacts. Human impacts are modeled. Climate impacts are estimated by subtracting modeled human impacts from GRACE trends. Negative values indicate a negative contribution to GMSL, slowing the rate of sea level rise.

mm/yr	*This Study*				*Other Studies*			
	Trend	*Source*	*Trend*	*Source*	*Trend*	*Source*	*Trend*	*Source*
GRACE (H+C)	-0.23	1	-0.20	2	-0.33	5	-0.29	6
Human (Model)	0.15	3	0.24	4	0.38	7	0.12	8
Climate (G - H)	-0.38		-0.44		-0.71		-0.41	
Glaciers					0.65	5	0.38	6
Ice sheets					1.26	5	0.99	6
Thermal expansion							1.38	6

Sources of data include: GRACE (human [H]) + climate [C]) from 1. CSR-M and 2. JPL-M (Table 3), human impacts from models 3. WGHM and 4. PCR-GLOBWB (Table 3), and climate contribution estimated by subtracting human impacts from GRACE trends. Other studies include GRACE trends from 5. Reager et al. (67), and 6. Rietbroek et al. (75), and human impacts from IPCC (68), and Wada et al. (69). The other components of the sea level budget are also shown for context, including land glaciers, ice sheets (Greenland and Antartica) and thermal expansion of the oceans. The net result from Rietbroek is a sea level rise of 2.68 mm/yr after including an additional 0.22 mm/yr (termed other component).

References

1. Cleveland RB, Cleveland WS, McRae JE, & Terpenning I (1990) STL: A seasonal-trend decomposition procedure based on loess. *J. Official Statistics* 6(1):3-73.
2. Humphrey V, Gudmundsson L, & Seneviratne SI (2016) Assessing global water storage variability from GRACE: trends, seasonal cycle, subseasonal anomalies and Eextremes. *Surveys in Geophysics* 37(2):357-395.
3. Scanlon BR*, et al.* (2016) Global evaluation of new GRACE mascons products for hydrologic applications. *Water Resour. Res.* 52(12):9412-9429.
4. Save H, Bettadpur S, & Tapley BD (2016) High-resolution CSR GRACE RL05 mascons. *J. Geophys. Res.-Solid Earth* 121(10):7547-7569.
5. Watkins MM, Wiese DN, Yuan DN, Boening C, & Landerer FW (2015) Improved methods for observing Earth's time variable mass distribution with GRACE using spherical cap mascons. *Journal of Geophysical Research-Solid Earth* 120(4):2648-2671.
6. Wiese DN (2015) GRACE monthly global water mass grids netcdf release 5.0. ver. 5.0. po.daac, ca, usa.dataset accesseed (2016-02004)), http://grace.jpl.nasa.gov/, doi:10.5067/TEMSC-OCL05.
7. Wiese DN, Landerer FW, & Watkins MM (2016) Quantifying and reducing leakage errors in the JPL RL05M GRACE mascon solution. *Water Resour. Res.* 52.
8. Haddeland I*, et al.* (2014) Global water resources affected by human interventions and climate change. *Proceedings of the National Academy of Sciences of the United States of America* 111(9):3251-3256.
9. Bierkens MFP (2015) Global hydrology 2015: State, trends, and directions. *Water Resources Research* 51(7):4923-4947.
10. Sood A & Smakhtin V (2015) Global hydrological models: a review. *Hydrological Sciences Journal-Journal Des Sciences Hydrologiques* 60(4):549-565.
11. Wada Y & Bierkens MFP (2014) Sustainability of global water use: past reconstruction and future projections. *Environmental Research Letters* 9(10).
12. Döll P, Kaspar F, & Lehner B (2003) A global hydrological model for deriving water availability indicators: model tuning and validation. *Journal of Hydrology* 270(1-2):105-134.
13. Ek MB*, et al.* (2003) Implementation of Noah land surface model advances in the National Centers for Environmental Prediction operational mesoscale Eta model. *Journal of Geophysical Research-Atmospheres* 108(D22).
14. Koster RD & Suarez MJ (1994) The components of a SVAT scheme and their effects on a GCMs hydrological cycle. *Adv Water Resour* 17(1-2):61-78.
15. Koster RD & Suarez MJ (1996) Energy and water balance calculations in the Mosaic LSM. in *NASA Tech. Memo.* (NASA TM-104606), p 60.
16. Liang X, Lettenmaier DP, Wood EF, & Burges SJ (1994) A simple hydrologically based model of land-surface water and energy fluxes for general-circulation models *Journal of Geophysical Research-Atmospheres* 99(D7):14415-14428.
17. Dai YJ*, et al.* (2003) The Common Land Model. *Bull. Amer. Meteorol. Soc.* 84(8):1013-1023.
18. Rodell M*, et al.* (2004) The global land data assimilation system. *Bull. Am. Meteor. Soc.* 85(3):381-394.
19. Koster RD, Suarez MJ, Ducharne A, Stieglitz M, & Kumar P (2000) A catchment-based approach to modeling land surface processes in a general circulation model 1. Model structure. *J. Geophys. Res. Atmospheres* 105(D20):24809-24822.
20. Weedon GP*, et al.* (2014) The WFDEI meteorological forcing data set: WATCH Forcing Data methodology applied to ERA-Interim reanalysis data. *Water Resources Research* 50(9):7505-7514.

21. van Beek LP, Wada Y, & Bierkens MFP (2011) Global Depletion of Groundwater Resources and Its Contribution to Sea-Level Rise. *Fall AGU meeting 2011 Abs H14B-01*.
22. Wada Y*, et al.* (2010) Global depletion of groundwater resources. *Geophys. Res. Lett.* 37, L20402, doi:10.1029/2010GL044571.
23. Portmann FT, Siebert S, & Döll P (2010) MIRCA2000-Global monthly irrigated and rainfed crop areas around the year 2000: A new high-resolution data set for agricultural and hydrological modeling. *Global Biogeochemical Cycles* 24.
24. Siebert S & Döll P (2010) Quantifying blue and green virtual water contents in global crop production as well as potential production losses without irrigation. *Journal of Hydrology* 384(3-4):198-217.
25. de Graaf IEM, Sutanudjaja EH, van Beek LPH, & Bierkens MFP (2015) A high-resolution global-scale groundwater model. *Hydrology and Earth System Sciences* 19(2):823-837.
26. McDonald RI*, et al.* (2014) Water on an urban planet: Urbanization and the reach of urban water infrastructure. *Global Environmental Change-Human and Policy Dimensions* 27:96-105.
27. Siebert S, Henrich V, Frenken K, & Burke J (2013) Global map of irrigaiton areas, version 5. *Rheinische Friedrich-Wilhelms-University, Bonn, Germany / Food and Agriculture Organization of the United Nations, Rome, Italy*.
28. Alcamo J*, et al.* (2003) Development and testing of the WaterGAP 2 global model of water use and availability. *Hydrological Sciences Journal-Journal Des Sciences Hydrologiques* 48(3):317-337.
29. Siebert S*, et al.* (2005) Development and validation of the global map of irrigation areas. *Hydrology and Earth System Sciences* 9(5):535-547.
30. Döll P*, et al.* (2012) Impact of water withdrawals from groundwater and surface water on continental water storage variations. *J. Geodyn.* 59-60:143-156.
31. Derber JC, Parrish DF, & Lord SJ (1991) The new global operational analysis system at the National Meteorological Center *Weather Forecasting* 6:538-547.
32. Xie PP & Arkin PA (1997) Global precipitation: A 17-year monthly analysis based on gauge observations, satellite estimates, and numerical model outputs. *Bull. Am. Met. Soc.* 78(11):2539-2558.
33. Rodell M, Houser PR, Berg AA, & Famiglietti JS (2005) Evaluation of 10 methods for initializing a land surface model. *Journal of Hydrometeorology* 6(2):146-155.
34. Reynolds CA, Jackson TJ, & Rawls WJ (2000) Estimating soil water-holding capacities by linking the Food and Agriculture Organization soil map of the world with global pedon databases and continuous pedotransfer functions. *Water Resour. Res.* 36(12):3653-3662.
35. Sheffield J, Goteti G, & Wood EF (2006) Development of a 50-year high-resolution global dataset of meteorological forcings for land surface modeling. *Journal of Climate* 19(13):3088-3111.
36. Adler RF*, et al.* (2003) AThe Version 2 Global Precipitation Climatology Project (GPCP) Monthly Precipitation Analysis (1979-Present). *J. Hydrometeor.,* 4:1147-1167.
37. Chen F*, et al.* (1996) Modeling of land surface evaporation by four schemes and comparison with FIFE observations. *J. Geophys. Res. Atmos.* 101 (D3):7251-7268.
38. Ek M*, et al.* (2003) Implementation of NOAH land-surface model advances in the NCEP operational mesoscale Eta model. *J. Geophys. Res., GCIP/GAPP Special Issue*.
39. Koster RD & Suarez MJ (1996) The influence of land surface moisture retention on precipitation statistics. *J. Climate* 9(10):2551-2561.
40. Avissar R & Pielke RA (1989) A parameterization of heterogeneous land surfaces for atmospheric numerical models and its impact on regional meteorology *Monthly Weather Review* 117(10):2113-2136.
41. Sellers PJ, Mintz Y, Sud YC, & Dalcher A (1986) A simple biosphere model (SIB) for use within general-circulation models *Journal of the Atmospheric Sciences* 43(6):505-531.

42. Zhao RJ, Zhang YI, L.R. F, X.R. L, & Zhang QS (1980) The Xinanjiang model. *Hydrological Forecasting Proceedings Oxford Symposium, IASH 129, Oxford U.K., April 1980, pp 351–356*.
43. Liang X, Lettenmaier DP, & Wood EF (1996) One-dimensional statistical dynamic representation of subgrid spatial variability of precipitation in the two-layer variable infiltration capacity model. *Journal of Geophysical Research-Atmospheres* 101(D16):21403-21422.
44. Cherkauer KA & Lettenmaier DP (2003) Simulation of spatial variability in snow and frozen soil. *Journal of Geophysical Research-Atmospheres* 108(D22).
45. Dai YX*, et al.* (2003) The Common Land Model (CLM). *Bull. Amer. Meteor. Soc.* 84(8):1013-1023.
46. Bonan GB & Stillwell-Soller LM (1998) Soil water and the persistence of floods and droughts in the Mississippi River Basin. *Water Resour. Res.* 34(10):2693-2701.
47. Dai Y & Zeng Q-C (1997) A land surface model (IAP94) for climate studies, Part I: Formulation and validation in off-line experiments. *Adv. Atmos. Sci.* 14:433-460.
48. Oleson KW*, et al.* (2010) Technical Description of Version 4.0 of the Community Land Model (CLM), 266 pp., Boulder, Colo.
49. Oleson KW*, et al.* (2013) Technical Description of version 4.5 of the Community Land Model (CLM). Ncar Technical Note NCAR/TN-503+STR, National Center for Atmospheric Research, Boulder, CO, 422 pp, DOI: 10.5065/D6RR1W7M.
50. Niu GY, Yang ZL, Dickinson RE, & Gulden LE (2005) A simple TOPMODEL-based runoff parameterization (SIMTOP) for use in global climate models. *Journal of Geophysical Research-Atmospheres* 110(D21).
51. Niu GY, Yang ZL, Dickinson RE, Gulden LE, & Su H (2007) Development of a simple groundwater model for use in climate models and evaluation with Gravity Recovery and Climate Experiment data. *Journal of Geophysical Research-Atmospheres* 112(D7).
52. Viovy N (2013) CRUNCEP Data Set V5. [Available at http://dods.ipsl.jussieu.fr/igcmg/IGCM/BC/OOL/OL/CRU-NCEP/, accessed 2013-8-5.].
53. Clapp RB & Hornberger GM (1978) Empirical equations for some soil hydraulic properties. *Water Resour. Res.* 14(4):601-604.
54. Beven KJ & Kirby MJ (1979) A physically based variable contributing area model of basin hydrology. *Hydrol. Sci. Bull.* 24:43-69.
55. Stieglitz M, Ducharne A, Koster R, & Suarez M (2001) The impact of detailed snow physics on the simulation of snow cover and subsurface thermodynamics at continental scales. 2, 228–242. *J. Hydrometeor.* 2:228-242.
56. Houborg R, Rodell M, Li BL, Reichle R, & Zaitchik BF (2012) Drought indicators based on model-assimilated Gravity Recovery and Climate Experiment (GRACE) terrestrial water storage observations. *Water Resources Research* 48.
57. Scanlon BR*, et al.* (2015) Hydrologic implications of GRACE satellite data in the Colorado River Basin. *Water Resources Research* 51(12):9891-9903.
58. Wahr J, Swenson S, & Velicogna I (2006) Accuracy of GRACE mass estimates. *Geophysical Research Letters* 33(6).
59. Lawrence DM*, et al.* (2011) Parameterization Improvements and Functional and Structural Advances in Version 4 of the Community Land Model. *Journal of Advances in Modeling Earth Systems* 3.
60. Dobslaw H*, et al.* (2013) Simulating high-frequency atmosphere-ocean mass variability for dealiasing of satellite gravity observations: AOD1B RL05. *Journal of Geophysical Research-Oceans* 118(7):3704-3711.
61. Landerer FW & Swenson SC (2012) Accuracy of scaled GRACE terrestrial water storage estimates. *Water Resour. Res.* 48.

62. Long D, Scanlon BR, Longuevergne L, & Chen X (2015) Global analysis of approaches for deriving total water storage changes from GRACE satellites and implications for groundwater storage change estimation. *AGU Fall Meeting Abstract H44F-06*.
63. Peltier WR, Argus DF, & Drummond R (2015) Space geodesy constrains ice age terminal deglaciation: The global ICE-6G_C (VM5a) model. *Journal of Geophysical Research-Solid Earth* 120(1):450-487.
64. Paulson A, Zhong SJ, & Wahr J (2007) Inference of mantle viscosity from GRACE and relative sea level data. *Geophysical Journal International* 171(2):497-508.
65. A G, Wahr J, & Zhong SJ (2013) Computations of the viscoelastic response of a 3-D compressible Earth to surface loading: an application to Glacial Isostatic Adjustment in Antarctica and Canada. *Geophysical Journal International* 192(2):557-572.
66. Purcell A, Tregoning P, & Dehecq A (2016) An assessment of the ICE6G_C(VM5a) glacial isostatic adjustmentmodel. *Journal of Geophysical Research-Solid Earth* 121(5):3939-3950.
67. Reager JT*, et al.* (2016) A decade of sea level rise slowed by climate-driven hydrology. *Science* 351(6274):699-703.
68. Church JA, P.U. Clark, A. Cazenave, J.M. Gregory, S. Jevrejeva, A. Levermann, M.A. Merrifield, G.A. Milne, R.S. Nerem, P.D. Nunn, A.J. Payne, W.T. Pfeffer, D. Stammer and A.S. Unnikrishnan (2013) Sea Level Change. In: Climate Change 2013: The Physical Science Basis. Contribution of Working Group I to the Fifth Assessment Report of the Intergovernmental Panel on Climate Change [Stocker, T.F., D. Qin, G.-K. Plattner, M. Tignor, S.K. Allen, J. Boschung, A. Nauels, Y. Xia, V. Bex and P.M. Midgley (eds.)]. Cambridge University Press, Cambridge, United Kingdom and New York, NY, USA.
69. Wada Y*, et al.* (2016) Fate of water pumped from underground and contributions to sea-level rise. *Nature Climate Change* 6(8):777-782.
70. Harris I, Jones PD, Osborn TJ, & Lister DH (2014) Updated high-resolution grids of monthly climatic observations - the CRU TS3.10 Dataset. *International Journal of Climatology* 34(3):623-642.
71. Schneider U*, et al.* (2014) GPCC's new land surface precipitation climatology based on quality-controlled in situ data and its role in quantifying the global water cycle. *Theoretical and Applied Climatology* 115(1-2):15-40.
72. Mueller Schmied H*, et al.* (2014) Sensitivity of simulated global-scale freshwater fluxes and storages to input data, hydrological model structure, human water use and calibration. *Hydrol. Earth Syst. Sci.* 18(9):3511-3538.
73. Muller Schmied H*, et al.* (2016) Variations of global and continental water balance components as impacted by climate forcing uncertainty and human water use. *Hydrology and Earth System Sciences* 20(7):2877-2898.
74. Kruskal WH & Wallis WA (1952) Use of ranks in one-criterion variance analysis. Journal of the American statistical Association, 47(260), 583-621.
75. Rietbroek R, Brunnabend SE, Kusche J, Schroter J, & Dahle C (2016) Revisiting the contemporary sea-level budget on global and regional scales. *Proceedings of the National Academy of Sciences of the United States of America* 113(6):1504-1509.